INTERIOR PERMANENT MAGNET SYNCHRONOUS MOTOR DEMAGNETIZATION FAULT MODELING AND ANALYSIS BY USING DYNAMIC PHASORS MODEL

A Thesis
Submitted to the Graduate Faculty
of the
North Dakota State University
of Agriculture and Applied Science

By

Feng Guo

In Partial Fulfillment of the Requirements
for the Degree of
MASTER OF SCIENCE

Major Department:
Electrical and Computer Engineering

July 2014

Fargo, North Dakota

North Dakota State University
Graduate School

Title

INTERIOR PERMANENT MAGNET SYNCHRONOUS MOTOR DEMAGNETIZATION FAULT MODELING AND ANALYSIS BY USING DYNAMIC PHASORS MODEL

By

Feng Guo

The Supervisory Committee certifies that this ***disquisition*** complies with North Dakota State University's regulations and meets the accepted standards for the degree of

MASTER OF SCIENCE

SUPERVISORY COMMITTEE:

Rajesh Kavasseri
Chair

Na Gong

Sumathy Krishnan

Approved:

7/30/2014
Date

Scott C. Smith
Department Chair

ABSTRACT

Interior permanent magnet synchronous motor (IPMSM) has been widely used in hybrid electric vehicles (HEVs) since the high power density and efficiency. However, the primary drawback of IPMSM is the demagnetization phenomenon caused by the permanent magnets. Modeling of the demagnetization fault are important in developing and designing a protection system for the traction on HEVs, thus, an efficient and accurate IPMSM model for demagnetization fault simulation is necessary. By using the conventional dq0 IPMSM model, the current indicators of demagnetization fault are affected by noise which will cause inaccuracy of the simulation. For this reason, a dynamic phasors model of IPMSM is presented in this thesis. In this thesis, firstly, the dynamic phasors model of IPMSM is verified by using small-signal transient analysis for its stability. Secondly, the time-domain transient simulations of positive sequence currents are shown and compared to the conventional dq0 model with demagnetization fault.

TABLE OF CONTENTS

LIST OF TABLES

Table Page

LIST OF FIGURES

Figure Page

LIST OF SYMBOLS

B ..... Friction coefficient of load and the machine

B_m ..... Flux density of the permanent magnet

B_r ..... Remanence of permanent magnet materials

H_c ..... Coercivity of permanent magnet

H_g ..... Magnetic field strenth in air

H_m ..... Magnetic field strenth in magnet

I_a ..... Armature current

I_n ..... Negative sequence current

I_p ..... Positive sequence current

J ..... Moment of inertia of the load and machine combined

L_d ..... Inductance of d-axis

L_q ..... Inductance of q-axis

N_a ..... Number of armature coil turns

P ..... Number of pole pairs

R_s ..... Resistance of the stator windings

T_e ..... Electromagnetic torque

T_l ..... Load torque

f_{demag} ..... Rotor fault frequency

f_s ..... Fundamental frequency

i_a, i_b, i_c ..... Instantaneous phase current of the stator windings

i_d ..... D-axis current at steady-state

i_q ..... Q-axis current at steady-state

i_s ..... Stator current in state space

l_g ..... Length of air gap

l_m ..... Length of magnet

p ..... Differential operator, $\frac{d}{dt}$

v_d ..... D-axis voltage at steady-state

V_n ..... Negative sequence voltage

V_p ..... Positive sequence voltage

v_q ..... Q-axis voltage at steady-state

Ω_0 ..... Fundamental rotor speed

Ω_2 ..... 2^{nd} order harmonic rotor speed

δ ..... Preceding a variable indicates small-signal variation

$\lambda_{1...7}$ ..... Eigenvalues from 1 to 7

λ_d ..... Flux linkage in the d-axis

λ_m ..... Rotor magnets flux linkages

λ_q ..... Flux linkage in the q-axis

ρ ..... Saliency ratio

ω ..... Mechanical rotor speed

μ ..... Permeability of air

μ_o ..... Magnetic permeability of air

μ_r ..... Relative premeability of permanent magnet

CHAPTER 1. INTRODUCTION

1.1. Overview

Hybrid electric vehicles (HEVs) have proved themselves to be the most comparable economical choice with better performance than the conventional combustion engine vehicles throughout the years. The electric motor is one of the main technologies in designing an HEV system.

Different electric machines determine the differences of the traction applications in electric vehicles. DC motor has been well used since a couple of decades ago [1], because of its characteristics of easy control. However, the reliability of the brushes on DC motor is the main problem for being used in HEV system. Nowadays, the Brushless DC motor (BLDC), Induction motor (IM), Permanent Magnet Synchronous Motor (PMSM) and Switched Reluctance Motor (SRM) have been developed since the advent of the powerful switching devices. And these motors are well served in different traction systems of most electric vehicle for different purposes. Each type of motor has its own advantages and disadvantages as shown in Table 1 [2–5].

Table 1. Comparison of different electric motors

Machine Type	Advantages	Disadvantages
Brushless DC Motor (BLDC)	High reliability High speed-torque characteristics	High cost Low speed range
Induction Motor (IM)	High speed range High reliability Low cost	low power density Low efficiency Large size
PM Synchronous Motor (PMSM)	High power density and small size High efficiency	Limited speed range High cost
Switched Reluctance Motor (SRM)	High speed-torque characteristics High reliability Low cost	High torque ripples Low power density Low efficiency

1.2. Thesis Motivation

A PMSM is the first choice for the HEV system, because of the high torque density and efficiency and the relatively smaller size compare to the IM and SRM. Also, as the name indicates, the rotor of permanent magnet synchronous motor is made by permanent magnets, such as samarium cobalt, used for exciting the magnetic field of the motor. Instead of the rotor coils in induction machine, the PMSM so that has the smaller size than IM and SRM. The PMSM has better efficiency because of the absence of the rotor winding, and the PMSM also has good efficiency at low speed, which is one of the most important features for the HEV system.

However, due to the permanent magnets in the rotor, this also causes some drawbacks. The rotor may be affected for many reasons that cause demagnetization. For example, when the motor runs above the rated speed, the high temperature will cause the demagnetization of permanent magnets in the rotor. Additionally, the failure of cooling system, and the aging of the magnets will also cause the demagnetization faults. Demagnetization of permanent magnets may significantly reduce the output torque, the efficiency of the PMSM, and even cause the irretrievable demagnetization. During the development of HEV traction system, the modeling of PMSM and simulation are the important parts. Thus, a reliable and efficiency modeling system is necessary, which could help in preventing damage of the motor, lengthen the lifespan, and reduce maintenance.

There has been much research to detect the demagnetization fault in permanent magnet synchronous motor. The most well-known one is the motor current signature analysis (MCSA) [6–11]. This method is based on fast Fourier transform (FFT) analyzing the stator current frequency spectrum according to

$$f_{demag} = f_s \left(1 \pm \frac{k}{P}\right) \qquad k = 1, 2, 3, ... \tag{1}$$

where f_{demag} and f_s are the rotor fault and fundamental frequency components, P is the number of pole pairs. Specific harmonics in the stator current spectrum can be detected as a specific type of fault. However, this method can be used when the motor is operating continuously in a nonstationary state. Discrete Fourier transform does not have the information about time [12]. Shout-time Fourier transform (STFT) can be applied to overcome the drawback between time and frequency. The limitations of selecting a suitable window size may cause an inconsistent treatment of different current frequencies [13, 14]. Therefore, it is difficult to detect the fault with very slow changes.

Time-frequency analysis such as wavelet transform [15–17] and also Hilbert-Huang transform (HHT) [18] were presented to solve these problems. However, the current spectrum indications may be covered by signal noise and the torque ripples. The limitations of these frequency analysis based methods are effected much by the spectrum caused by the current noise.

To inject a signal into the motor is one the method to detect the PM demagnetization [19]. The signal is injected to the motor only when the motor is at standstill. The machine model-based methods detect the positive/negative sequence currents [20], or monitoring the zero sequence voltage [21]. These indicators are sensitive to machine faults and also have lower cost. However, the indicators (positive/negative sequence currents, etc.) are affected by torque ripples and current noise, which will affect the accuracy. Thus it is very important to be able to accurately and efficiently model PMSM in electric vehicle system simulations.

Although there are several modeling of PMSM and IM by using dynamic phasors model [22–24], none of the models presented in the literature take into account of demagnetization fault modeling and effect to the traction system, and where the modeling and simulation of the traction systems are the vital step in developing

electric vehicles. To summarize, the main motivations of this research for designing a new online modeling system are:

- Find a model that can be used for significantly fast simulations of transient when demagnetization fault occurs;
- Model the motor conditions in both stationary and nonstationary situations, and monitor the effect of demagnetization fault to the PMSM;
- Increase the sensitivity and accuracy of the fault detections;
- Reduce the cost, and shorten the calculation speed.

In the next section of this chapter, permanent magnet materials and different types of PMSM are presented.

1.3. Permanent Magnet Materials

The modern permanent magnets started to be considered to develop the PM field excitation in the 1950s [25]. Various materials, such as Alnico-5, ferrites, samarium-cobalt, and neodymium-boron-iron are developed as permanent magnets of the PM machines. In the present, the PM machines are widely used in industry because of the well development of the high quality of permanent magnet materials.

Figure 1. is a typical curve of a permanent magnet material, this curve is one of the material samples, different materials have different slope of the curve.

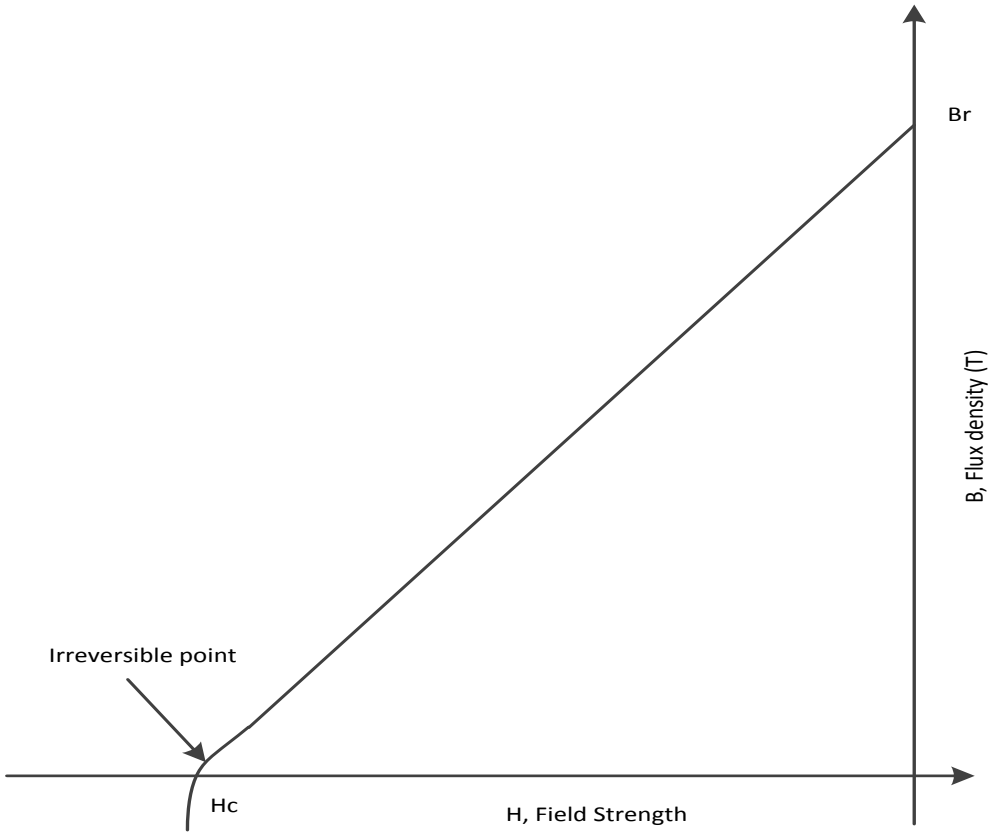

Figure 1. B-H characteristics of permanent magnets

B_r is the remanence of the permanent magnet material, which is the flux density at zero excitation, H_c is coercivity which is the negative field strength that brings the remanence to zero, and the slope of the curve is called permeability. From Figure 1., the flux density at zero excitation is known as remnant flux density B_r, and when the machine is operation around the knee point, the flux density will go to zero. If the external excitation acting against the magnet is removed, and the operation point is above the knee point, the magnet will recover along the B-H curve back to B_r [26].

1.4. Operating Point of the PMSM

To simulate the demagnetization fault of PMSM, we need to find out the relationship between the field strength and the flux density that the permanent magnet has. Firstly, we need to find the operating point on the demagnetization fault on the magnet.

From Ampere's law, the permeance coefficient line is shown in equation [27–29]

$$B_m = \mu_o \frac{A_g}{l_g A_m} \left(-H_m l_m + N_a I_a\right) \tag{2}$$

where μ is the permeability of air, H_m and H_g are magnetic field strengths in magnet and air, respectively, and l_m and l_g are the length of the magnet and air gap. N_a is the number of armature coil turns and I_a is the armature current. This line is shown in Figure 2. The demagnetization curve shown in Figure 1. can be approximated as

$$B_m = B_r + \mu_o \mu_r H_m \tag{3}$$

where $\mu_o \mu_r$ is the slope of the demagnetization curve in Figure 2.

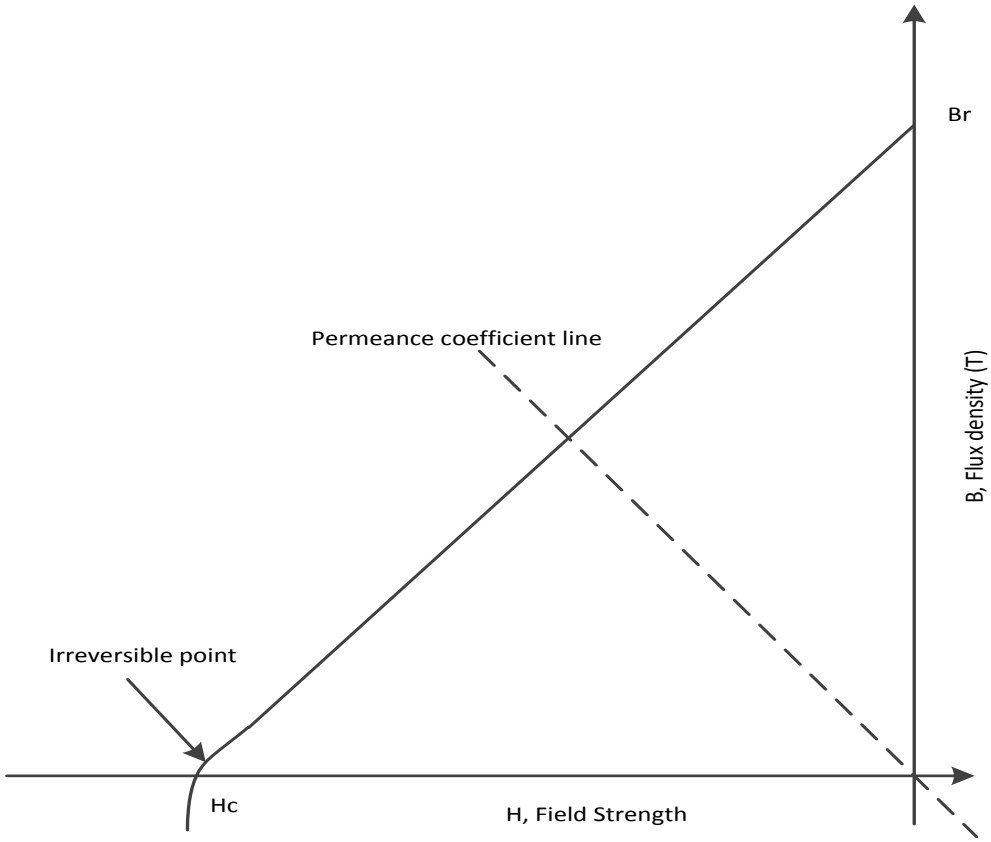

Figure 2. Demagnetization curve and operating point

From permeance coefficient line equation (2), for operating an electric machine, the current is less than zero. Thus, the permeance coefficient line (dash line) in Figure 2. moves to the left, so that the flux density is reduced. This operation is called demagnetization. If the permeance coefficient line moves over the knee point of the demagnetization curve (solid line), the permanent magnet is irreversible damaged. For this reason, the online monitoring of the permanent magnets demagnetization is necessary in most of the applications.

1.5. Interior Permanent Magnet Synchronous Motor (IPMSM)

With the development of permanent magnet materials and the techniques of driving an electric machine, the usage of the PMSM has rapidly increased in many areas, especially in the applications of electric vehicle because of the advantages in efficiency and size.

The PMSM has a three-phase stator winding, and a rotor with permanent magnets for field excitation. Normally, the PMSM is the name of surface-mounted permanent magnet synchronous motor (SPMSM), where the permanent magnets are attached at the surface of the rotor. In this type of motor, the rotation speed is limited in order to keep the permanent magnets attached on the surface. For this reason, in the present, most of HEV systems are using interior permanent magnet synchronous motor (IPMSM) in the traction systems.

This type of motor has permanent magnets inside of the rotor and has the same operating principal as SPMSM. And there are also several types of IPMSM in structures, and each one has its own advantages. Figure 3. shows the basic rotor structures of SPMSM and one of the rotor structures of IPMSM.

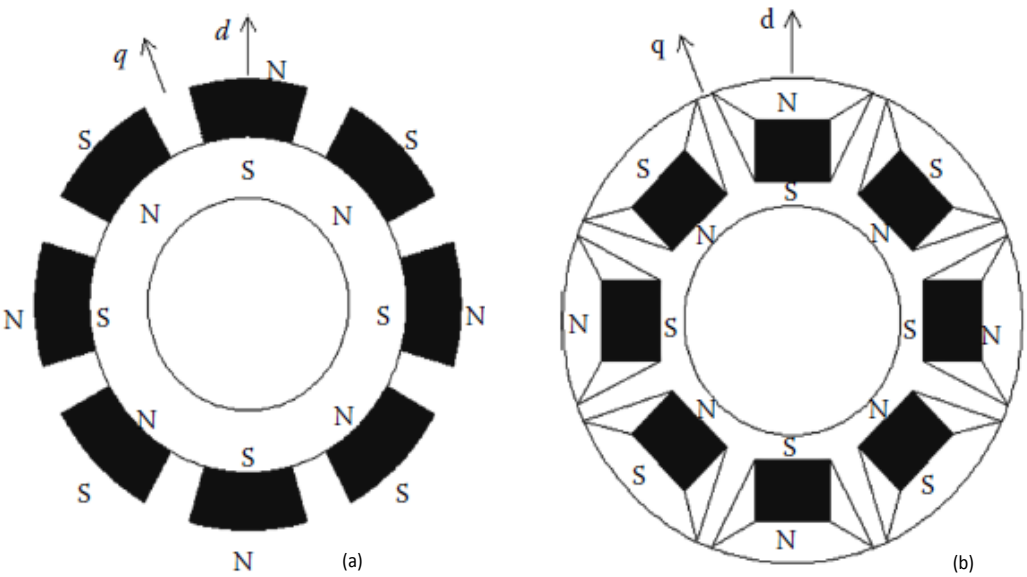

Figure 3. The rotor structures of (a) SPMSM and (b) IPMSM [26]

The parameters of structure (a) and (b) shown in Figure 3. are used as conventional PMSM and IPMSM respectively in Chapter 5 for modeling and comparison.

CHAPTER 2. CONCEPT OF DYNAMIC PHASORS

The concept of phasors is based on the property that a periodic time-domain waveform $x(\tau)$ with period T, that is $x(\tau) = x(\tau - T)$, can be expressed as a complex Fourier series of the form

$$x(\tau) = \sum_{k=-\infty}^{\infty} X_k \cdot e^{jk\omega_s \tau} \tag{4}$$

where $\omega_s = 2\pi/T$ and X_k is the k^{th} Fourier coefficient in complex form. In this case, since $x(\tau)$ is periodic, the Fourier coefficient X_k are time invariant and can be expressed as

$$X_k = \frac{1}{T} \int_{t-T}^{t} x(\tau) e^{-jk\omega_s \tau} d\tau \tag{5}$$

2.1. Single Phase Systems

To generalize equations (4, 5) to accommodate arbitrary, nearly periodic types of waveforms. We need to use the property mentioned in [30], where the Fourier coefficients are allowed to vary with time. Considering a window of length T for the waveform of interest, and viewing that waveform to be periodic with a duration of T, such that a Fourier analysis of the waveform $x(\tau)$ can be performed. The time evolution of the Fourier coefficients can be calculated as the window of length T.

Now for any time-domain waveform $x(\tau)$ with period T can be represented on the interval $\tau \in (t - T, t]$ using a Fourier series of the form

$$x(\tau) = \sum_{k=-\infty}^{\infty} X_k \cdot e^{jk\omega_s \tau} \tag{6}$$

where these Fourier coefficients are functions of time since the interval under consideration slides as a function of time. So that the k^{th} coefficient at time t is determined

by the following averaging operation

$$X_k = \frac{1}{T}\int_{t-T}^{t} x(\tau)e^{-jk\omega_s\tau}d\tau = \langle x\rangle_k(t) \tag{7}$$

Some useful properties of the Fourier coefficients that will be used in later chapters. When original waveforms $x(\tau)$ are complex-valued, the phasor

$$X_k = \langle x\rangle_{\_}\, k = \langle x^*\rangle_k \tag{8}$$

where * is the complex conjugate. In the case where $x(\tau)$ is real valued, the equation is reduced to $X_k = X_k^*$

The time derivative for the k^th Fourier coefficient can be obtained by differentiating equation (4) with respect to time.This key property can be expressed as

$$\frac{dX_k}{dt} = \left\langle \frac{dx}{dt} \right\rangle_k - jk\omega_s X_k \tag{9}$$

2.2. PolyPhase Systems

The goal in this chapter is to implement the dynamic phasors concept to 3-phase Permanent Magnet Synchronous Motor, so that we need to extend the dynamic phasor concept to include polyphase systems. We begin by using the method symmetrical components which allows a set of unbalanced phasors to be expressed as the sum of n symmetrical sets of balanced phasors. In this thesis, we consider three phase (a-b-c) case. Therefore, the phasors representing an unbalanced three-phase set can be expressed in three terms, (1) balanced set of phasors with an abc sequence (positive sequence), (2) balanced set of phasors with an acb sequence (negative sequence), and (3) a set of three equal phasors (zero sequence). Figure 4. gives the illustration of the tree sets of balanced sequence components.

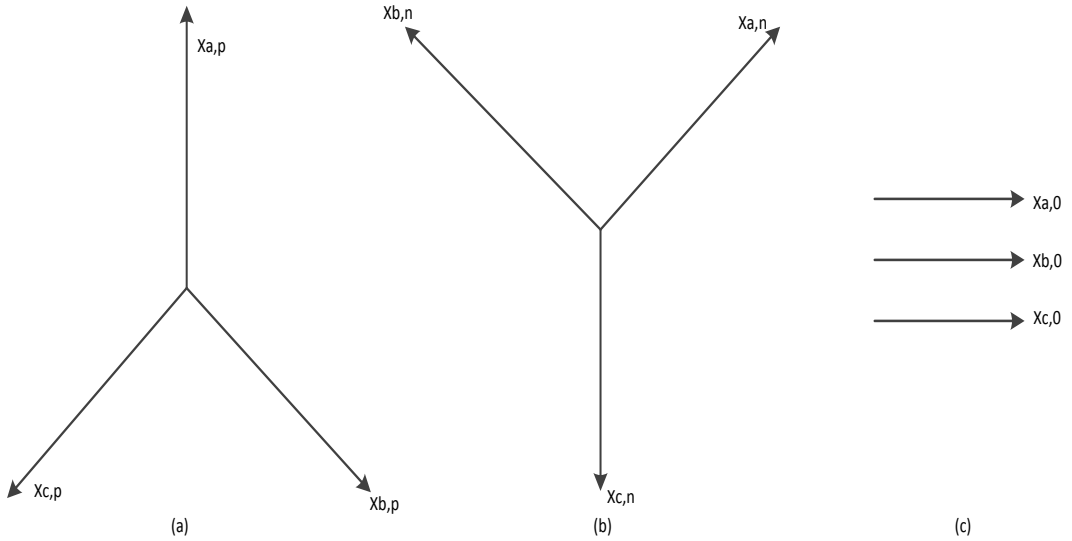

Figure 4. (a). Positive (b). Negative (c). Zero sequence components

The transformation is introduced following the standard notation, $\alpha = e^{j(2\pi/3)}$; then $\alpha^2 = \alpha^*$. Then a time-domain waveform can be written as

$$\begin{bmatrix} x_a \\ x_b \\ x_c \end{bmatrix} = \begin{bmatrix} 1 & 1 & 1 \\ \alpha^2 & \alpha & 1 \\ \alpha & \alpha^2 & 1 \end{bmatrix} \begin{bmatrix} X_{a,p} \\ X_{a,n} \\ X_{a,0} \end{bmatrix} \tag{10}$$

where $\alpha^2 = e^{j(4\pi/3)} = e^{-j(2\pi/3)}$. The inverse transformation is given as follows

$$\begin{bmatrix} X_{a,p} \\ X_{a,n} \\ X_{a,0} \end{bmatrix} = 1/3 \begin{bmatrix} 1 & 1 & 1 \\ \alpha^2 & \alpha & 1 \\ \alpha & \alpha^2 & 1 \end{bmatrix} \begin{bmatrix} x_a \\ x_b \\ x_c \end{bmatrix} \tag{11}$$

Using the transformation in equation (10) and extending the single phase dynamic phasors principles outlined in Section 2.1 to the polyphase system, we can

express three phase time domain dynamic phasors equation

$$\begin{bmatrix} x_a \\ x_b \\ x_c \end{bmatrix}(\tau) = \sum_{k=-\infty}^{\infty} e^{jk\omega_s\tau} M \begin{bmatrix} X_{p,k} \\ X_{n,k} \\ X_{0,k} \end{bmatrix}(t) \tag{12}$$

the Fourier coefficients in equation (12) are

$$\begin{bmatrix} X_{p,k} \\ X_{n,k} \\ X_{0,k} \end{bmatrix}(t) = \frac{1}{T} \int_{t-T}^{t} e^{-jk\omega_s\tau} M^{-1} \begin{bmatrix} x_a \\ x_b \\ x_c \end{bmatrix}(\tau)d\tau = \begin{bmatrix} \langle x \rangle_{p,k} \\ \langle x \rangle_{n,k} \\ \langle x \rangle_{0,k} \end{bmatrix}(t) \tag{13}$$

The Fourier coefficients in equation (13) represent the dynamic phasors of the positive-sequence $X_{p,k}$, negative-sequence $X_{n,k}$ and zero-sequence $X_{0,k}$ components of the time varying signals represented in equation (12)

After applying the same properties mentioned in Section 2.1 for the single phase dynamic phasors, the polyphase equation (12) is a vector form for the three-phase case. The coefficients in (12) are

$$\frac{d}{dt}\begin{bmatrix} X_{p,k} \\ X_{n,k} \\ X_{0,k} \end{bmatrix}(t) = M^{-1} \begin{bmatrix} \left\langle \frac{d}{dt}x_a(\tau) \right\rangle_k \\ \left\langle \frac{d}{dt}x_b(\tau) \right\rangle_k \\ \left\langle \frac{d}{dt}x_c(\tau) \right\rangle_k \end{bmatrix}(t) - jk\omega_s \begin{bmatrix} X_{p,k} \\ X_{n,k} \\ X_{0,k} \end{bmatrix}(t) \tag{14}$$

We also have the relationship between balanced sequence components shown as

$$\begin{bmatrix} \langle x \rangle_{p,k} \\ \langle x \rangle_{n,k} \\ \langle x \rangle_{0,k} \end{bmatrix} = \begin{bmatrix} \langle x^* \rangle^*_{p,-k} \\ \langle x^* \rangle^*_{n,-k} \\ \langle x^* \rangle^*_{0,-k} \end{bmatrix}(t) - jk\omega_s \begin{bmatrix} X_{p,k} \\ X_{n,k} \\ X_{0,k} \end{bmatrix}(t) \tag{15}$$

2.3. Dynamic Phasors and Complex Space Vectors

The method of symmetrical components has been used to analyze unbalanced operation of symmetrical electric machines. For the complex space vectors, there is a transformation of the three-phase variables to a stationary complex reference frame, which combine the qd equations into a single complex expression. That is, since the qd axes are orthogonal, it is

$$\overrightarrow{f}_{qds} = f_{qs} - jf_{ds} \tag{16}$$

this equation can be used for instantaneous phasor, so that equation (16) is important in deriving the dynamic phasors system in the next chapter.

It is common to introduce the concept of complex space vectors. The stator consists of three sinusoidally currents that are 120° apart from one another. Then we can have a relationship shown as [31]

$$\overrightarrow{x}(t)_{qds} = \frac{2}{3}(x_a(t) + \alpha x_b(t) + \alpha^* x_c(t)) \tag{17}$$

The α in equation (17) is the same as that in the previous section, which is $\alpha = e^{j(2\pi/3)}$. Since stator current phasor have the same magnitude and 120° apart from one another, we have

$$i_{as} + i_{bs} + i_{cs} = 0 \tag{18}$$

when zero-sequence is zero, the phase current can be represented as

$$\overrightarrow{i}_{abcs} = i_{as} - \frac{1}{2}(i_{bs} + i_{cs}) + j\frac{\sqrt{3}}{2}(i_{bs} - i_{cs}) = i_{as} + j\frac{\sqrt{3}}{2}(i_{bs} - i_{cs}) \tag{19}$$

From equation (19), there is a simple inverse transformation

$$i_a s = \mathbf{R}(\overrightarrow{i}_{abcs}) \tag{20}$$

$$i_b s = \mathbf{R}(\alpha^* \overrightarrow{i}_{abcs}) \tag{21}$$

$$i_c s = \mathbf{R}(\alpha \overrightarrow{i}_{abcs}) \tag{22}$$

$$\tag{23}$$

where $\mathbf{R}$ denotes the real part of a complex number.

From equation (6, 19), we can implement the dynamic phasors concept to express to complex space vectors [31], then we can get

$$\overrightarrow{x}(\tau) = \frac{2}{\sqrt{3}} \sum_{k=-\infty}^{\infty} e^{jk\omega_s \tau} X_{p,k}(\tau) \tag{24}$$

In equation (19) the variable 'x' was specified to stator current in this thesis. Since all phase quantities are real-value, we have $X_{p,-k} = X^*_{n,k}$. When zero-sequence components are zero, and $\overrightarrow{x}$ represents the information about positive and negative sequence quantities. In this thesis, $k = \pm 1$

$$\overrightarrow{x}(\tau) = X_{p,k}(\tau) e^{j\omega_s \tau} + X^*_{n,k}(\tau) e^{-j\omega_s \tau} \tag{25}$$

CHAPTER 3. DYNAMIC PHASORS MODEL OF IPMSM

3.1. Dynamic Modeling of Permanent Magnet Synchronous Machines

The Permanent Magnet Synchronous Machine is consisted of two parts, stator with supplied source, and a rotor with only permanent magnets. The dynamic model of the permanent magnet synchronous machine (IPMSM) is derived using a two-phase motor in direct and quadrature axes. The magnets are modeled as a constant current source, concentrating all its flux linkages along only one axis. In this thesis, the inductance versus rotor position is assumed to be sinusoidal, and the saturation and parameter changes are neglected. A two-phase IPMSM stator with windings and rotor with PMs is shown in Figure. It is assumed that the q-axis leads the d-axis.

The transient voltage equivalent circuit can be defined in d-q axes in the rotor reference frames,

$$\begin{aligned} v_d &= R_s i_d + pL_d i_d - \omega\lambda_q \\ v_q &= R_s i_q + pL_q i_q + \omega\lambda_d \end{aligned} \tag{26}$$

The stator and rotor flux linkages in rotor reference frames are defined as

$$\lambda_q = L_q i_q \tag{27}$$

$$\lambda_d = L_d i_d + \lambda_m \tag{28}$$

where λ_q, λ_d are the flux linkage in the d-q axes, λ_m is the rotor magnets flux linkages, and p is the operation of $\frac{d}{dt}$.

Base on the stator equations, the equivalent circuit of IPMSM can be derived and shown as Fig.5. The equivalent circuits are

- Dynamic stator q-axis equivalent circuit
- Dynamic stator d-axis equivalent circuit

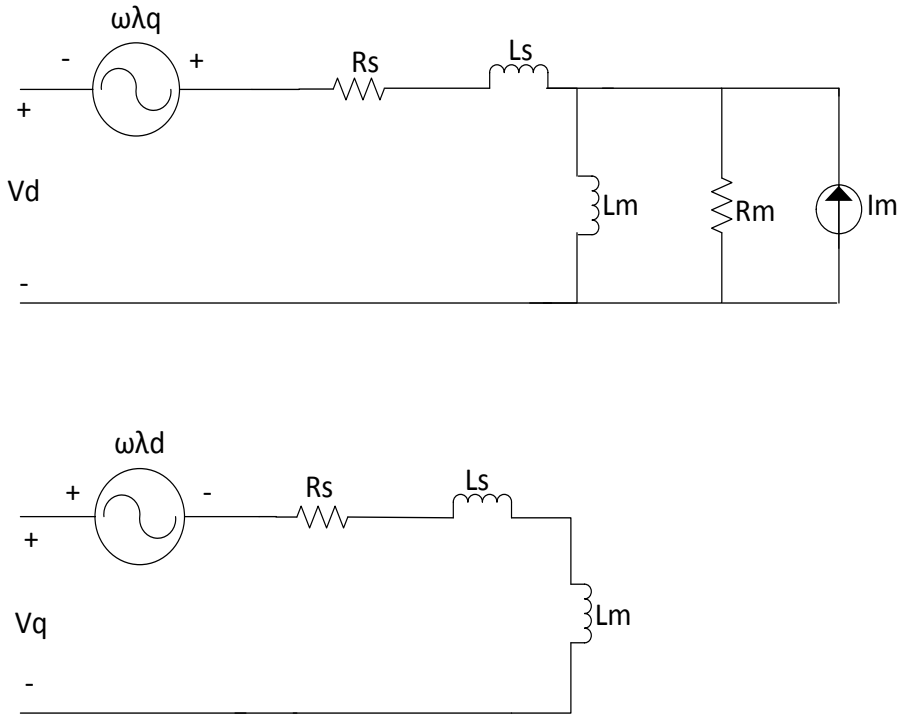

Figure 5. Equivalent circuit of dq0 model of IPMSM

In this thesis, the core losses are not the most concern, so that the core losses are neglected in these equivalent circuits.

In the equivalent model of IPMSM, the rotor magnet can be considered as a loop of constant current source like the excitation on an induction motor rotor. This provides a way to relate the calculation of the demagnetization current for the magnet. In the first chapter, the flux linkage is proved to be proportional to the demagnetization of the PMs, thus, the current source here in the equivalent is also proportional to the demagnetization. Then in the process of simulation, the different demagnetization faults can be generated by changing the value λ_m. The equivalent

current source is derived as [32]

$$I_m = \frac{4\sqrt{2}}{3\pi}\frac{PB_r l_m}{\mu_o \mu_r N_a} sin\beta \tag{29}$$

where β is one-half of the magnet arc.

The electromagnetic torque as a function of the flux linkages is defined as

$$T_e = \frac{3}{2}\frac{P}{2}\frac{1}{L_q}[\rho\lambda_m + (1-\rho)\lambda_d]\lambda_q = \frac{3}{2}\frac{P}{2}[\lambda_d i_q - \lambda_q i_d] \tag{30}$$

where the saliency ratio is defined as

$$\rho = \frac{L_q}{L_d} \tag{31}$$

The negative sign in equation (30) shows that the d-axis current produces a counter torque to the machine.

The electromechanical dynamic equation is given by

$$T_e = J\frac{d\omega_m}{dt} + T_l + B\omega \tag{32}$$

where,

ω is the mechanical rotor speed,

J is the moment of inertia of the load and machine combined, B is the friction coefficient of the load and the machine, and T_l is the load torque.

3.2. Dynamic Phasors Model of IPMSM

Now we have all the basic knowledge of IPMSM and dynamic phasors procedures prepared in previous sections, we need to derive the IPMSM model into dynamic phasors model. The dq0 axes model of permanent magnet synchronous machine is defined in equation (27). And space vector dynamic model in the rotor coordinate

frame can be derived by using equation (16). Then we can get [31]

$$\begin{aligned}
\overrightarrow{v}_s &= \overrightarrow{v}_q - j\overrightarrow{v}_d \\
&= (R_s + \frac{L_d + L_q}{2}(j\omega\frac{P}{2} + \frac{d}{dt}))\overrightarrow{i}_s + \frac{L_q - L_d}{2}(j\omega\frac{P}{2} + \frac{d}{dt})\overrightarrow{i}_s^* + \omega\frac{P}{2}\lambda_m \qquad (33) \\
J\frac{d}{dt}\omega &= \frac{2P}{8}\frac{j}{2}(L_q - L_d)((\overrightarrow{i}_s)^2 - (\overrightarrow{i}_s^*)^2) + \frac{2P}{8}\lambda(\overrightarrow{i}_s + \overrightarrow{i}_s^*) - B\omega - T_l
\end{aligned}$$

where the subscript s corresponds to stator quantities and the superscript r corresponds to rotor reference frame.

The dynamic phasors model of permanent magnet synchronous machine can be developed by applying equation (9, 25) to the complex space vector model in equation (33). Since the zero sequence quantities are zero, there are only positive and negative sequence present. Then we can get the dynamic phasors model in the following equation systems (34), (35). Since the torque ripple caused by unbalanced conditions, both dc component of the rotor speed Ω_0 and the second order harmonic rotor speed Ω_2 are considered.

$$\begin{aligned}
V_p &= (R_s + \frac{L_d + L_q}{2}(j\Omega_0\frac{P}{2} + \frac{d}{dt}))I_p + \frac{3j}{2}\Omega_2^*\frac{P}{2}\frac{L_q - L_d}{2}I_n \\
&\quad + \frac{L_q - L_d}{2}(\frac{j}{2}\Omega_0\frac{P}{2} + \frac{d}{dt})I_p^* - j\Omega_2\frac{P}{2}\frac{L_d + L_q}{2}I_n^* + \Omega_0\frac{P}{2}\lambda_m \qquad (34) \\
V_n &= (R_s + \frac{L_d + L_q}{2}(j\Omega_0\frac{P}{2} + \frac{d}{dt}))I_n - \frac{j}{2}\Omega_2\frac{P}{2}\frac{L_q - L_d}{2}I_p \\
&\quad - j\Omega_2\frac{P}{2}\frac{L_q + L_d}{2}I_p^* + \Omega_2\frac{P}{2}\lambda_m
\end{aligned}$$

The mechanical equation can be expressed for PMSM in terms of dynamic phasors as shown below.

$$\begin{aligned}
J\frac{d}{dt}\Omega_0 &= \frac{3P}{j8}(\frac{L_q - L_d}{2}((I_p)^2 - (I_p^*)^2)) + \frac{3P}{j8}\lambda_m(I_p + I_p^*) - B\Omega_0 - T_l \qquad (35) \\
J\frac{d}{dt}\Omega_2 &= \frac{3P}{j8}((L_q + L_d)I_p^*I_n + \lambda_m I_n) - (B + j2J\Omega_0\frac{P}{2})\Omega_2
\end{aligned}$$

From equations above, each equation are coupled and there are λ_m terms in each equation except the fundamental speed dynamic equation (Ω_0) in equation (35). And the permanent flux linkage is proportional to the magnetic strength as mentioned in previous chapter. This means that this dynamic phasors model of IPMSM has the direct relationship with permanent magnet flux linkage, so that this model allows us to observe the system when demagnetization fault happens. We now have all the dynamic phasors equations needed in order to implement to the model to IPMSM demagnetization fault detections. We can see in dynamic phasors model (34),35), these are all nonlinear equations, some of the terms are the products of two current variables or a current variable and rotor speed. To check the stability of the system when demagnetization fault appears, we need to use eigenvalue analysis method. However, the nonlinear dynamic equations cannot be directly used, the small signal transient analysis is used here and will be introduced in detail in the next chapter.

CHAPTER 4. EIGENVALUE ANALYSIS

The dynamic phasors model of permanent magnet synchronous machine given in (34), (35) give the dynamic equations of the entire motor-load system. These dynamic equations are nonlinear, which is not directly applicable for eigenvalue analysis. They have to be linearized around an operating point by using perturbation techniques [9]. The ideal model to get the linearized model is the one with steady-state operating-state variables. By using these steady-state operating-state values as dc value, and plus a small signal perturbation, we can get the linearized variables.

The voltage, current, torque and rotor speed in their steady state are denoted in $v_o, i_o, T_o, and\omega_o$, and the perturbed increments are demoted by a δ. Then all the variables after perturbation are

$$v_q = v_{qo} + \delta v_q \tag{36}$$

$$v_d = v_{do} + \delta v_d \tag{37}$$

$$i_q = i_{qo} + \delta i_q \tag{38}$$

$$i_d = i_{do} + \delta i_d \tag{39}$$

$$T = T_o + \delta T \tag{40}$$

$$\omega = \omega_o + \delta\omega \tag{41}$$

By substituting from equations (36) to equations (34, 35), by neglecting the second-order terms, and by canceling the steady-state terms on both right and left hand sides of the equations, the small signal dynamic equations can be obtained.

After linearizing the dynamic phasors model by using small signal method, we can get a linearized model with seven equations. Including both real and image parts

of positive sequence voltage, negative sequence voltage and second-order harmonic rotor speed, and only one equation for fundamental rotor speed since this variable is the only real value. All the including variables are denoted as $\mathbf{Re}(I_p), \mathbf{Im}(I_p), \mathbf{Re}(I_n), \mathbf{Im}(I_n)$, $\Omega_0, \mathbf{Re}(\Omega_2)$ and $\mathbf{Im}(\Omega_2)$, respectively.

$$
\begin{aligned}
-L_q\frac{d}{dt}\delta Re(I_p) =& R_s\delta Re(I_p) + (k_2-k_3)\Omega_{0o}\delta Im(I_p) + (k_1+k_3)Im(\Omega_{2o})\delta Re(I_n) \\
&- (k_1+k_3)Re(\Omega_{2o})\delta Im(I_n) + ((k_2-k_3)Im(I_{po}) + \frac{P}{2}\lambda)\delta\Omega_0 \\
&- (k_1+k_3)Im(I_{no})\delta Re(\Omega_2) + (k_1+k_3)Re(I_{no})\delta Im(\Omega_2) - Re(V_{po}) \\
-L_d\frac{d}{dt}\delta Im(I_p) =& (k_2+k_3)\Omega_{0o}\delta Re(I_p) + R_s\delta Im(I_p) + (k_1-k_3)Re(\Omega_{2o})\delta Re(I_n) \\
&+ (k_1-k_3)Im(\Omega_2 o)\delta Im(I_n) + (k_2+k_3)Re(I_{po})\delta\Omega_{0o} \\
&+ (k_1-k_3)Re(I_{no})\delta Re(\Omega_2) + (k_1-k_3)Im(I_{no})\delta Im(\Omega_2) - Im(V_{po}) \\
-\frac{k_4}{2}\frac{d}{dt}\delta Re(I_n) =& (k_2+k_3)Im(\Omega_{2o})\delta Re(I_p) + (k_2-k_3)Re(\Omega_{2o})\delta Im(I_p) \\
&+ R_s\delta Re(I_n) - k_3\Omega_{0o}\delta Im(I_n) - k_3Im(I_{no})\delta\Omega_0 + ((k_2-k_3)Im(I_{po}) \\
&+ \frac{P}{2}\lambda)\delta Re(\Omega_2) + (k_2+k_3)Re(I_{po})\delta Im(\Omega_2) - Re(V_n) \\
-\frac{k_4}{2}\frac{d}{dt}\delta Im(I_n) =& -(k_2+k_3)Re(\Omega_{2o})\delta Re(I_p) + (k_2-k_3)Im(\Omega_{2o})\delta Im(I_p) \\
&+ k_3\Omega_{0o}\delta Re(I_n) + + R_s\delta Im(I_n) + k_3Re(I_{no})\delta\Omega_0 \\
&- (k_2+k_3)Re(I_{po}))\delta Re(\Omega_2) + ((k_2-k_3)Im(I_{po}) + \frac{P}{2}\lambda)\delta Im(\Omega_2) \\
&- Im(V_{no}) - Im(V_n) \\
J\frac{d}{dt}\delta\Omega_0 =& k_6Im(I_{po})\delta Re(I_p) + k_5Re(I_{po})\delta Im(I_p) - B\delta\Omega_0
\end{aligned}
$$

$$
\begin{aligned}
J\frac{d}{dt}\delta Re(\Omega_2) =& k_6 Im(I_{no})\delta Re(I_p) - k_6 Re(I_{no})\delta Im(I_p) - k_6 Im(I_{po})\delta Re(I_n) \\
&+ (k_6 Re(I_{po}) + \frac{3P}{8}\lambda)\delta Im(I_n) + JPIm(\Omega_{2o})\delta\Omega_0 - B\delta Re(\Omega_2) \\
&+ JP\Omega_{0o}\delta Im(\Omega_2) \\
J\frac{d}{dt}\delta Im(\Omega_2) =& - k_6 Re(I_{no})\delta Re(I_p) - k_6 Im(I_{no})\delta Im(I_p) - (k_6 Re(I_{po}) + \frac{3P}{8}\lambda)\delta Re(I_n) \\
&- k_6 Im(I_{po})\delta Im(I_n) - JPRe(\Omega_{2o})\delta\Omega_0 - B\delta Im(\Omega_2) - JP\Omega_{0o}\delta Re(\Omega_2)
\end{aligned} \tag{42}
$$

Now the nonlinear systems (34, 35) are linearized by reducing the order of the dynamic equations to equations (42). To find the eigenvalue of this small signal system, we need to cast the equation system (42) into state-space form gives

$$
px = Ax + Bu \tag{43}
$$

where

$$
x = \begin{bmatrix} \delta Re(I_p) & \delta Im(I_p) & \delta Re(I_n) & \delta Im(I_n) & \delta\Omega_0 & \delta Re(\Omega_2) & \delta Im(\Omega_2) \end{bmatrix}^T \tag{44}
$$

$$
u = \begin{bmatrix} \delta Re(V_p) & \delta Im(V_p) & \delta Re(V_n) & \delta Im(V_n) & \delta T_l & 0 & 0 \end{bmatrix}^T \tag{45}
$$

and system matrix $A = U^{-1}M$, $B = U^{-1}W$

$$U = \begin{bmatrix} -k_7 & 0 & -k_8 & 0 & 0 & 0 & 0 \\ 0 & -k_7 & 0 & k_8 & 0 & 0 & 0 \\ 0 & 0 & -k_7 & 0 & 0 & 0 & 0 \\ 0 & 0 & 0 & -k_7 & 0 & 0 & 0 \\ 0 & 0 & 0 & 0 & J & 0 & 0 \\ 0 & 0 & 0 & 0 & 0 & J & 0 \\ 0 & 0 & 0 & 0 & 0 & 0 & J \end{bmatrix} \tag{46}$$

$$M = \begin{bmatrix} M_{11} & M_{12} & M_{13} \\ M_{21} & M_{22} & M_{23} \\ M_{31} & M_{32} & M_{33} \end{bmatrix} \tag{47}$$

where,

$$M_{11} = \begin{bmatrix} R_s & (k_2 - k_3)\Omega_{0o} \\ (k_2 + k_3)\Omega_{0o} & R_s \end{bmatrix}$$

$$M_{12} = \begin{bmatrix} (k_1 + k_3)Im(\Omega_{2o}) & -(k_1 + k_3)Re(\Omega_{2o}) \\ (k_1 - k_3)Re(\Omega_{2o}) & (k_1 - k_3)Im(\Omega_{2o}) \end{bmatrix}$$

$$M_{13} = \begin{bmatrix} (k_2 - k_3)Im(I_{po}) + \frac{P}{2}\lambda & -(k_1 + k_3)Im(I_{no}) & (k_1 + k_3)Re(I_{no}) \\ (k_2 + k_3)Re(I_p) & (k_1 - k_3)Re(I_n) & (k_1 - k_3)Im(I_n) \end{bmatrix}$$

$$M_{21} = \begin{bmatrix} (k_2 + k_3)Im(\Omega_{2o}) & (k_2 - k_3)Re(\Omega_{2o}) \\ -(k_2 + k_3)Re(\Omega_{2o}) & (k_2 - k_3)Im(\Omega_{2o}) \end{bmatrix}$$

$$M_{22} = \begin{bmatrix} R_s & -k_3\Omega_{0o} \\ k_3\Omega_{0o} & R_s \end{bmatrix}$$

$$M_{23} = \begin{bmatrix} -k_3 Im(I_{no}) & (k_2 - k_3)Im(I_{po}) + \frac{P}{2}\lambda & (k_2 + k_3)Re(I_{po}) \\ k_3 Re(I_{no}) & -(k_2 + k_3)Re(I_{po}) & (k_2 - k_3)Im(I_{po}) + \frac{P}{2}\lambda \end{bmatrix}$$

$$M_{31} = \begin{bmatrix} k_5 Im(I_{po}) & k_5 Re(I_{po}) \\ k_6 Im(I_{no}) & -k_6 Re(I_{no}) \\ -k_6 Re(I_{no}) & -(k_6 Re(I_{po}) + \frac{3P}{8}\lambda) \end{bmatrix}$$

$$M_{32} = \begin{bmatrix} 0 & 0 \\ -k_6 Im(I_{po}) & k_6 Re(I_{po}) + \frac{3P}{8}\lambda \\ -(k_6 Re(I_{po}) + \frac{3P}{8}\lambda) & -k_6 Im(I_{po}) \end{bmatrix}$$

$$M_{33} = \begin{bmatrix} -B & 0 & 0 \\ JPIm(\Omega_{2o}) & -B & JP\Omega_{0o} \\ -JPRe(\Omega_{2o}) & -JP\Omega_{0o} & -B \end{bmatrix}$$

and,

$$W = diag \begin{bmatrix} 1 & 1 & 1 & 1 & 1 & 0 & 0 \end{bmatrix}$$

where

$$k_1 = \frac{3}{2}\frac{P}{2}\frac{L_q - L_d}{2}, \qquad k_2 = \frac{1}{2}\frac{P}{2}\frac{L_q - L_d}{2}, \qquad k_3 = \frac{P}{2}\frac{L_q + L_d}{2}$$
$$k_4 = \frac{L_q + L_d}{2}, \qquad k_5 = \frac{3P}{2}\frac{L_q - L_d}{2}, \qquad k_6 = \frac{3P}{8}k_4$$
$$k_7 = \frac{k_4}{2} \qquad k_8 = \frac{L_q - L_d}{2}$$

Base on the system matrix A, it is apparent that the IPMSM dynamic phasors model has seven eigenvalues. In the system matrix A, the magnet flux linkage can be changed to simulate the demagnetization fault since the proportional relationship with the magnetic strength. The parameters been used are shown in Table 2.

Table 2. Rated parameters of IPMSM

Parameters	Values
Volt. (V)	285
$R_s(\Omega)$	1.4
$L_d(mH)$	5.7
$L_q(mH)$	9
$L_m(mH)$	154.6
Pole pairs	6
J $(kg.m^2)$	0.0012
B	0.1

The eigenvalue analysis has been done on different rating of demagnetizations. The eigenvalues of IPMSM dynamic model at both full-load and no-load operating points are shown in Table 3.

Table 3. The eigenvalues on different demagnetization percentages

Mag. percentage %		eigenvalues (full-load)	eigenvalues (no-load)
100%	$\lambda_{1,2}$	$-37.2 \pm i1852.5$	$-28.4 \pm i1879.4$
	$\lambda_{3,4}$	$-145.4 \pm i926.6$	$-151.9 \pm i928.5$
	$\lambda_{5,6}$	$-246.0 \pm i885.2$	$-248.8 \pm i883.5$
	λ_7	-8.4	-8.3
80 %	$\lambda_{1,2}$	$-30.0 \pm i1851.6$	$-22.0 \pm i1880.9$
	$\lambda_{3,4}$	$-148.5 \pm i927.6$	$-154.4 \pm i929.2$
	$\lambda_{5,6}$	$-250.0 \pm i883.8$	$-252.7 \pm i880.6$
	λ_7	-8.4	-8.4
70%	$\lambda_{1,2}$	$-26.8 \pm i1850.8$	$-18.7 \pm i1882.4$
	$\lambda_{3,4}$	$-149.5 \pm i928.0$	$-155.5 \pm i929.2$
	$\lambda_{5,6}$	$-251.9 \pm i883.0$	$-254.6 \pm i878.4$
	λ_7	-8.4	-8.4
60%	$\lambda_{1,2}$	$-23.2 \pm i1846.4$	$-17.0 \pm i1883.4$
	$\lambda_{3,4}$	$-150.0 \pm i929.7$	$-156.2 \pm i926.4$
	$\lambda_{5,6}$	$-254.3 \pm i883.1$	$-255.3 \pm i876.2$
	λ_7	-8.5	-8.5
50%	$\lambda_{1,2}$	$447.8 \pm i1242.9$	$312.5 \pm i1455.7$
	$\lambda_{3,4}$	$-660.4 \pm i839.7$	$-523.6 \pm i920.8$
	$\lambda_{5,6}$	$-164.0 \pm i681.0$	$-179.4 \pm i782.9$
	λ_7	-91.9	-73.9

From these group of eigenvalues, the eigenvalues $\lambda_{1,2}$ correspond to the second harmonic rotor speed Ω_2, and λ_7 correspond to the fundamental rotor speed Ω_0, where $\lambda_{3,4}$ and $\lambda_{5,6}$ are positive sequence and negative sequence currents. It shows

that the permanent magnets demagnetization has the effect to all the eigenvalues when the machine runs in stable range. From 40% to 50% demagnetization, the machine becomes unstable since the first pairs of eigenvalues $\lambda_{1,2}$ are positive. For detail representation, the eigenvalues of the 2^{nd} order harmonic rotor speed Ω_2 of IPMSM between 40% and 50% are plotted in Fig. 6. The demagnetization changes the machine system, which is system matrix A. In this case, the eigenvalues are plotted out by changing the system matrix A, and keep the system input the same, which is the operating point at the stable situation.

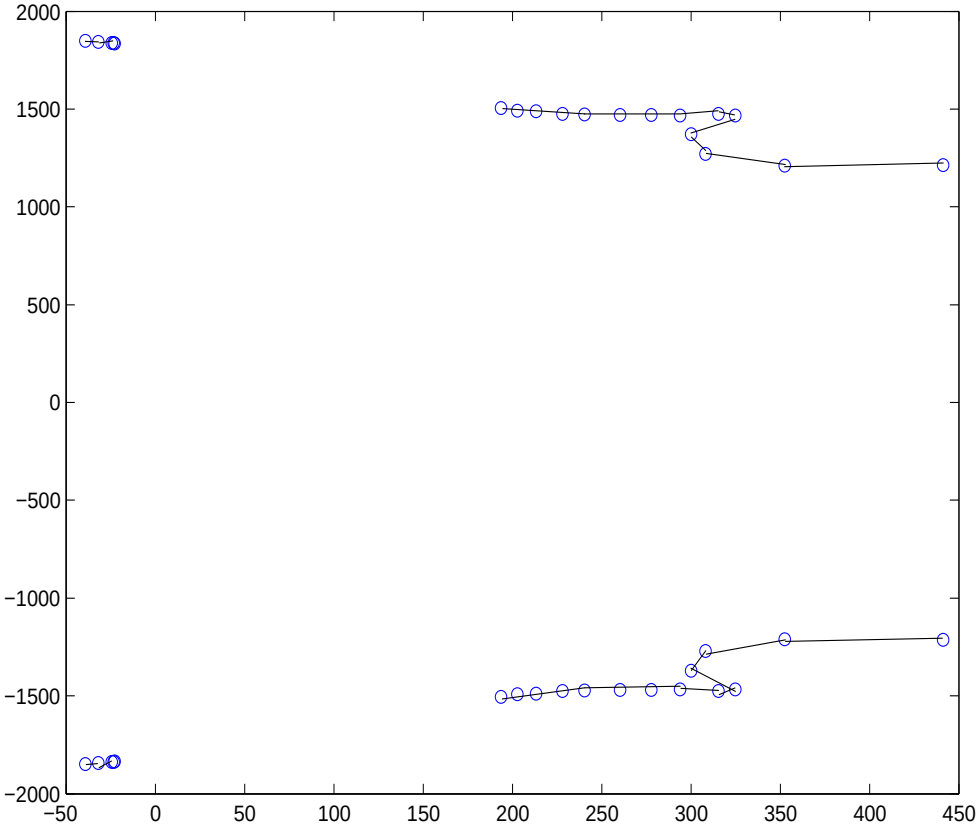

Figure 6. Eigenvalues correspond to 2^{nd} order harmonic speed ($\lambda_{1,2}$)

The eigenvalues $\lambda_{1,2}$ move to positive side along with the demagnetization percentage increase. It is important to note that between 43% to 44% demagnetizations, the eigenvalue trace is discontinued. The system goes to unstable at this moment. Above 44% demagnetization, the system goes to unstable as eigenvalue trace shows in Figure 6.

The eigenvalues $\lambda_{3...7}$ are remained negative between 40% to 50% demagnetization of the permanent magnets. For more clear showing in the figures, the eigenvalues correspond to the demagnetization less than 40% are neglected in Figure 7.,8. The details of the eigenvalues are shown in the following figures.

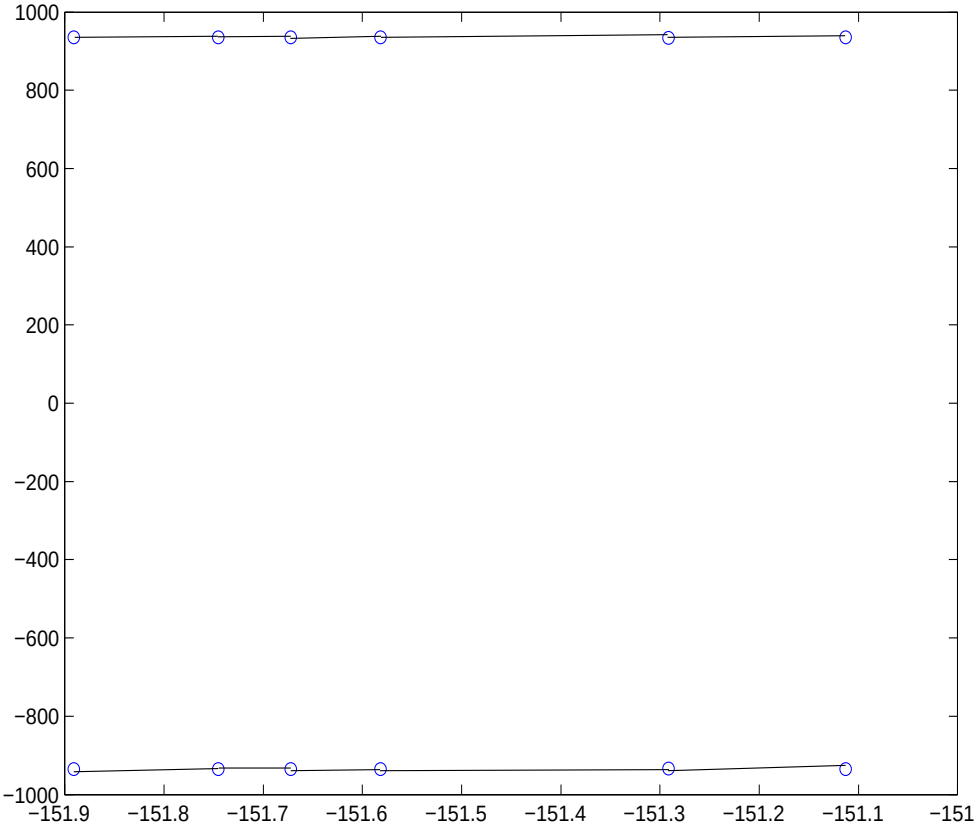

Figure 7. Eigenvalues correspond to positive sequence current ($\lambda_{3,4}$)

Eigenvalues $\lambda_{3,4}$ move towards positive side of the x-axis because of the demagnetization fault, and the eigenvalue traces are smooth between these points.

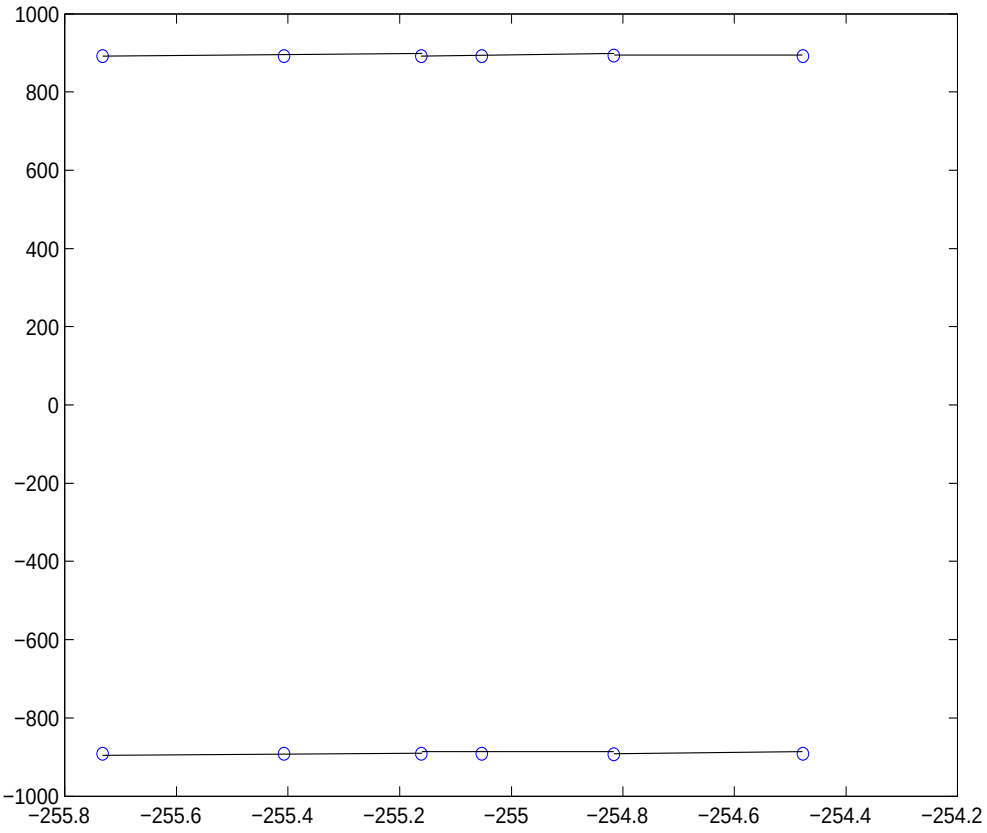

Figure 8. Eigenvalues correspond to negative sequence current ($\lambda_{5,6}$)

Eigenvalues $\lambda_{5,6}$ move towards positive side of the x-axis because of the demagnetization fault.

For detail representations, the eigenvalues of both healthy and faulted machine are plotted in Figure 9.,10. and 11., for different loading from no-load to full-load. In the entire range of loading conditions, the eigenvalues are almost proportional effected. From 56% demagnetization, the eigenvalues shows that the system runs unstably. From no-load to full-load conditions, the eigenvalues move to positive side

to x-axis.

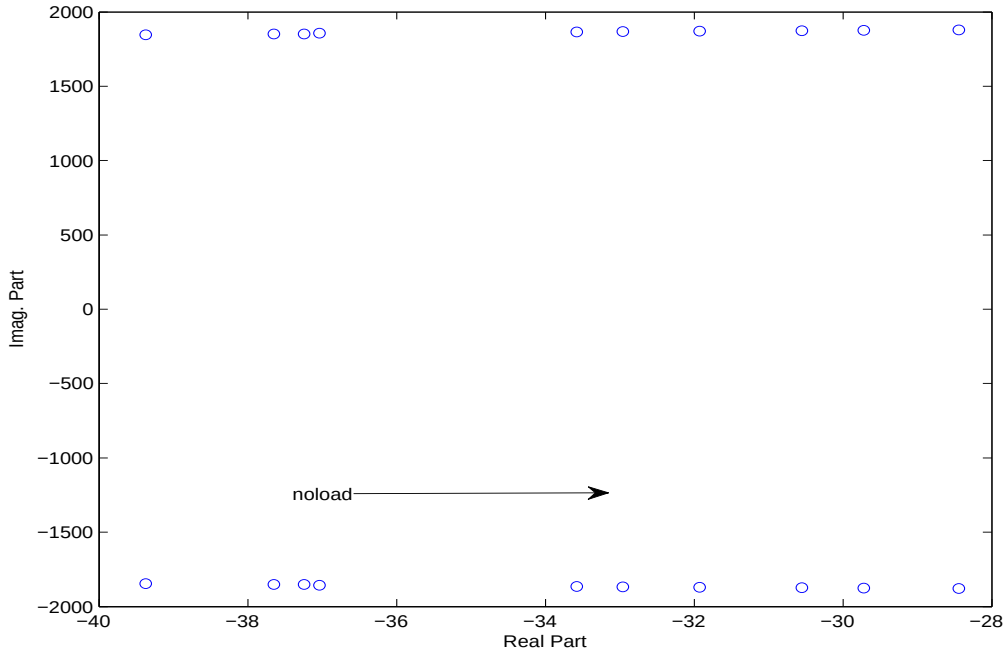

Figure 9. 2^{nd} order harmonic speed ($\lambda_{1,2}$) from no-load to full-load condition

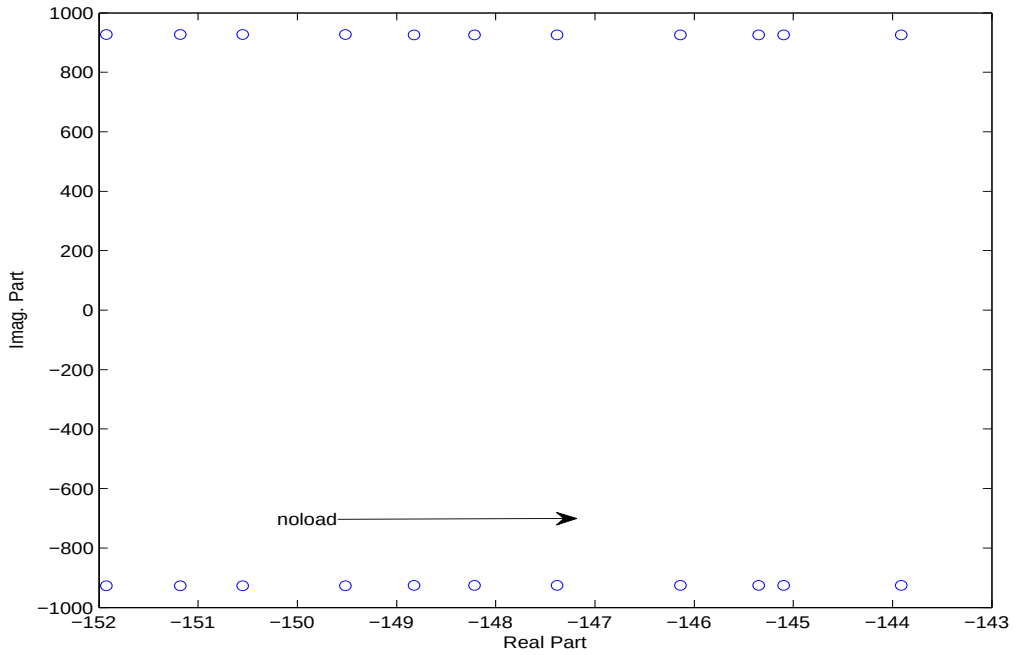

Figure 10. Positive sequence current ($\lambda_{3,4}$) from no-load to full-load condition

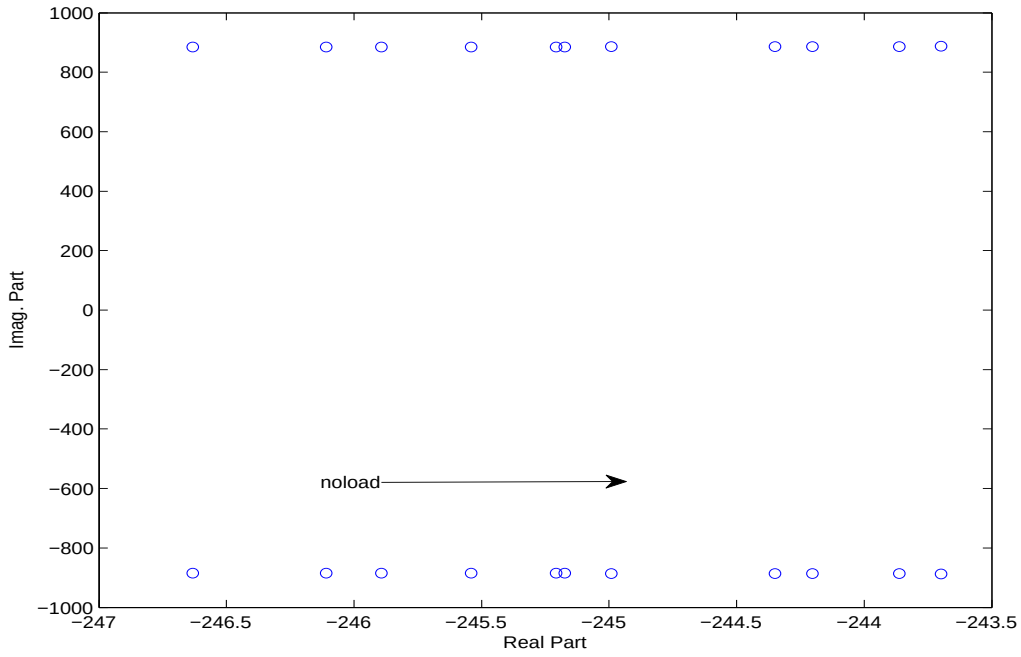

Figure 11. Negative sequence current ($\lambda_{5,6}$) from no-load to full-load condition

CHAPTER 5. RESULTS

The permanent magnet synchronous machine dynamic model was presented in Chapter 3, and was also verified the stability during the fault by using the eigenvalue analysis in Chapter 4. In this chapter, the performance of detecting the demagnetization faults using IPMSM dynamic phasors model will be shown. And also the comparison of dynamic phasors model and the conventional dq0 model will be given in section (4.2). A series of simulations are implemented to verify the dynamic phasors model represents the considerable results. In this chapter, the comparison between dq0 model and dynamic phasors model will be represented in different conditions, and the advantages of

- 1. faster calculation
- 2. less noise, more accuracy for detections

will be shown in details in the following sections.

5.1. Demagnetization Fault Modeling in Dynamic Phasors Model

The IPMSM dynamic phasors model was presented as equation (34), (35) in Chapter 3. This system has seven state variables ($\mathbf{Re}(I_p), \mathbf{Im}(I_p), \mathbf{Re}(I_n), \mathbf{Im}(I_n), \Omega_0$, $\mathbf{Re}(\Omega_2)$ and $\mathbf{Im}(\Omega_2)$). The simulation begins at time t=0s when a rated voltage 285V is applied to the motor with initial rotor speed runs at 326 rad/s. The following figures are the dynamic time domain plot of these seven state variables when the IPMSM is running at the stationary condition (constant speed). Figure 12. shows the motor runs at 326.5 rad/s. By using the same machine parameters as shown in Table 1, the IPMSM dynamic phasors model is simulated as following. Since the positive/negative sequence currents are sensitive to the motor faults, thus the analysis of I_p, I_n can shows the faults significantly. This chapter will be more focus on observing the positive and negative sequence values.

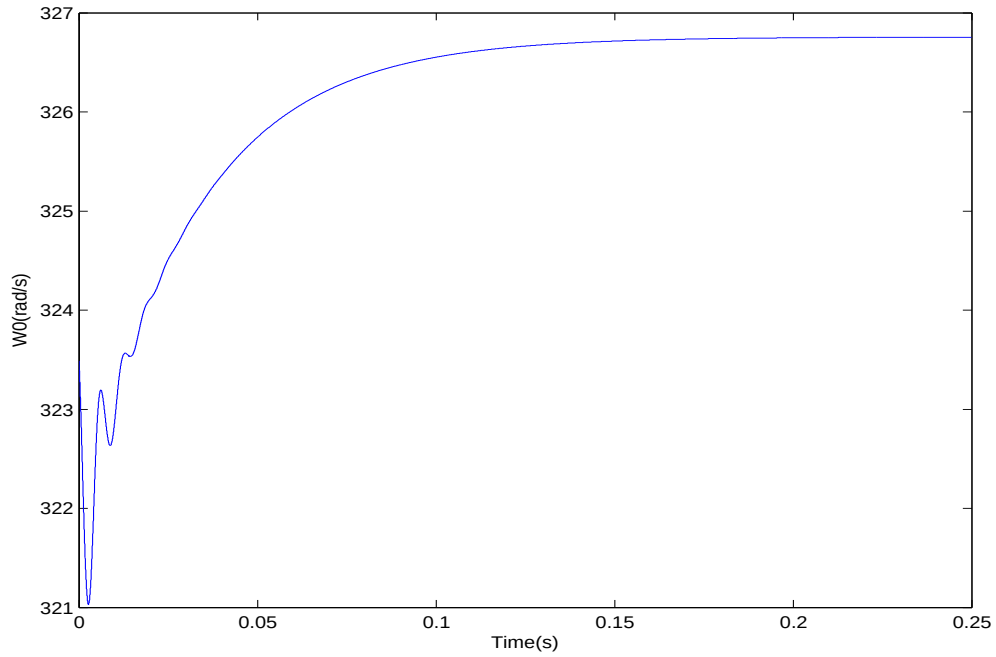

Figure 12. Fundamental rotor speed Ω_0 in dynamic phasors model

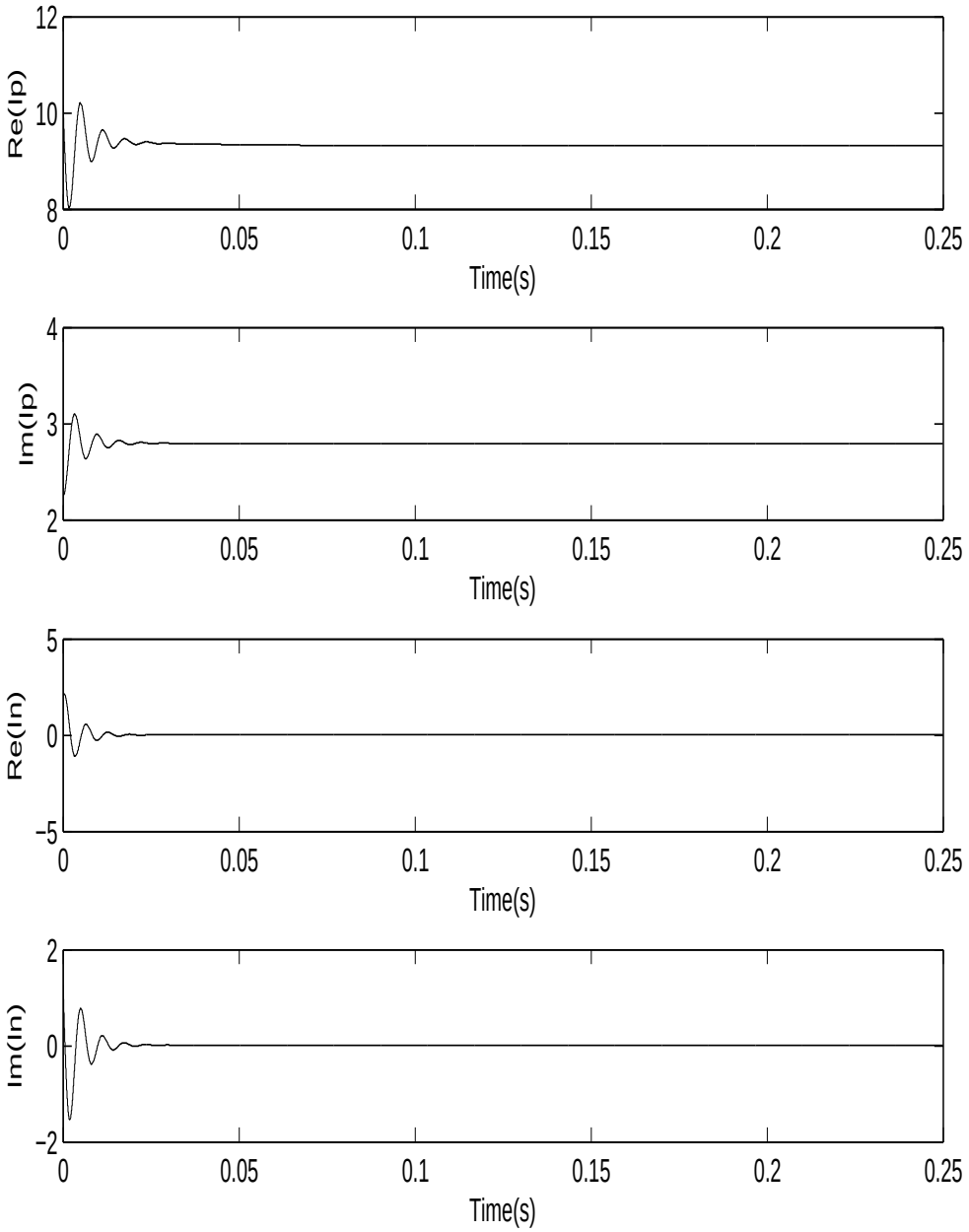

Figure 13. Complex value of positive and negative sequence current

Figure 13. shows both positive and negative sequence current are stabled in balanced condition, the negative sequence current is almost zero, since the supply

voltage is three-phase balanced. 2^{nd} order harmonic speed Ω_2 is shown in Figure 14.

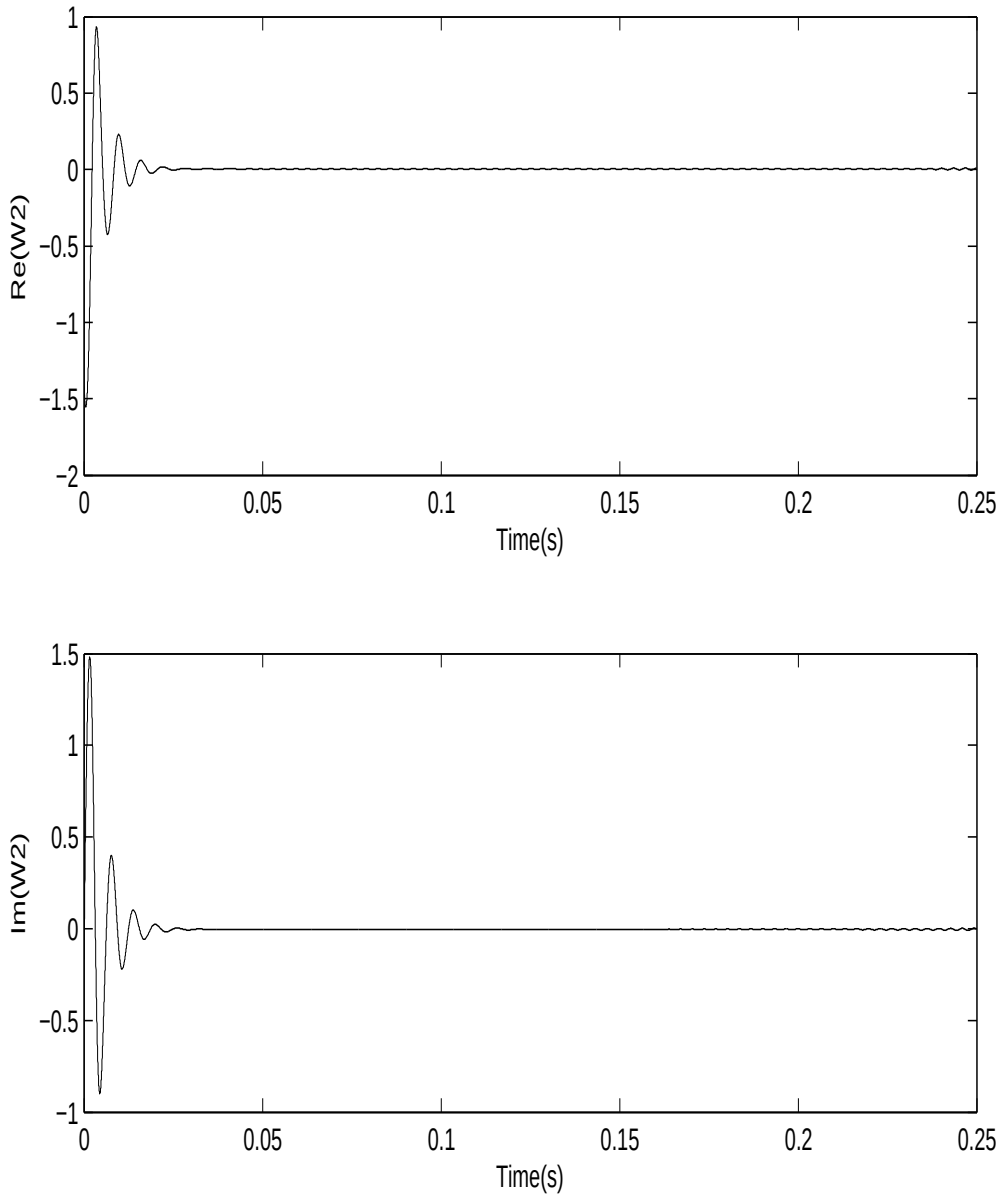

Figure 14. 2^{nd} order harmonic speed $\Omega_{1,2}$ in dynamic phasors model

The 2^{nd} order harmonic speed is zero since the output torque ripples are small during the stationary situation. This IPMSM dynamic phasors model is well verified

by both time domain transient and also eigenvalues analysis in previous chapter. Now it is the point that we need to use this dynamic phasors model to detect the demagnetization faults.

To simulate the uniform demagnetization, we can proportionally decrease the permanent magnets flux linkage λ_m. In the following figures, the demagnetization fault of IPMSM appeared at t=0.1s to t=0.15s, the positive sequence current I_p has obvious changes at this moment. The field excitation reduced, that means the back EMF in the stator winding are reduced, so that the three-phase stator current will increase. In the meantime, the positive sequence current will increase, as shown in Figure 15. Although the $Im(I_p)$ is decreased during the demagnetization fault, the magnitude of total positive sequence current is increased. The negative sequence current is around zero at this moment because of the motor runs balanced.

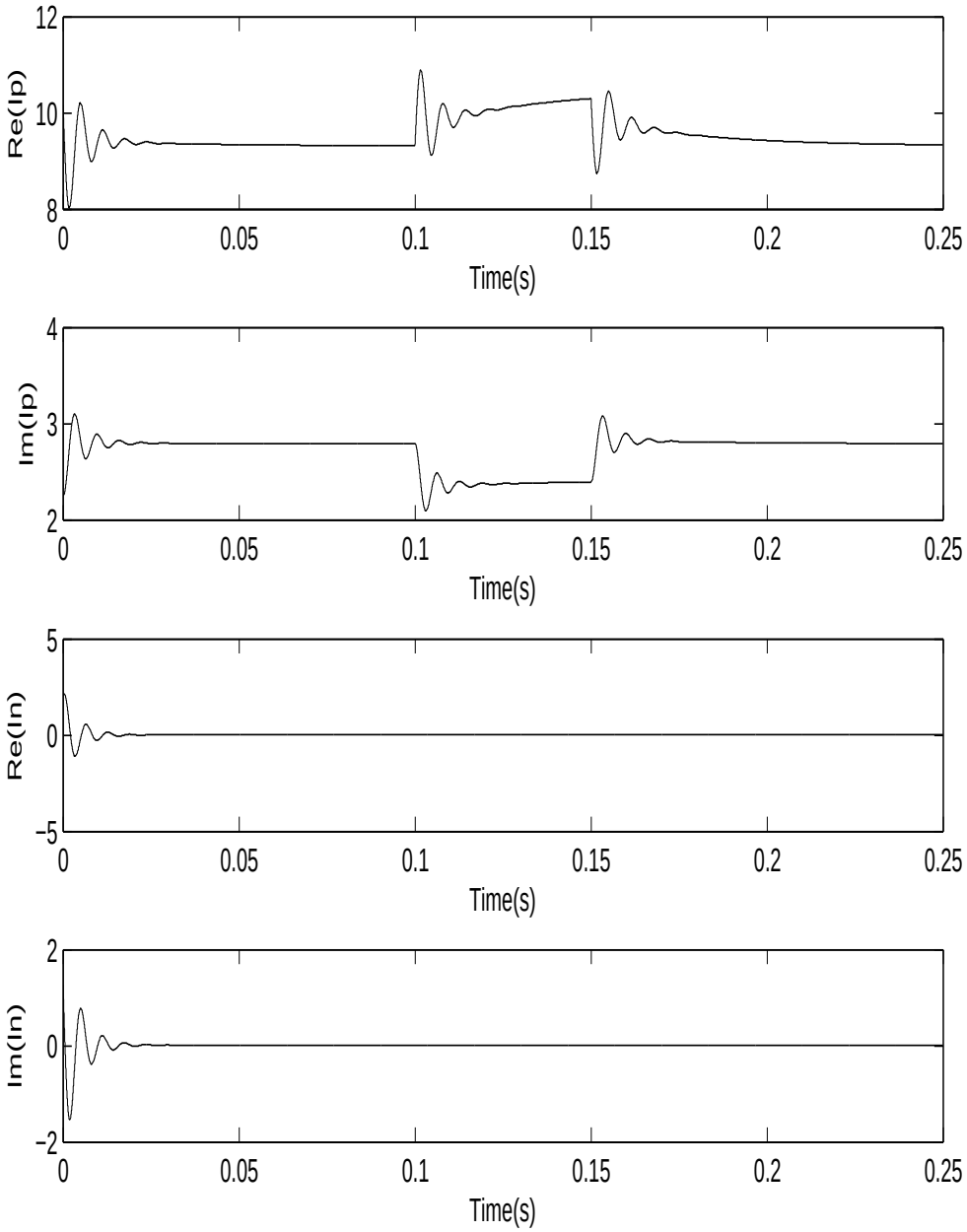

Figure 15. Positive and negative sequence current with 20% demagnetization fault

Also, in Figure 15.,the negative sequence current is shown as zero. Although the uniform demagnetization fault happens, the motor still runs balanced. In the

same reason, the 2^{nd} order harmonic speed $\Omega_{1,2}$ have very small transient start from t=0.1s because of the little ripples caused by demagnetization fault, and it is shown in Figure 16.

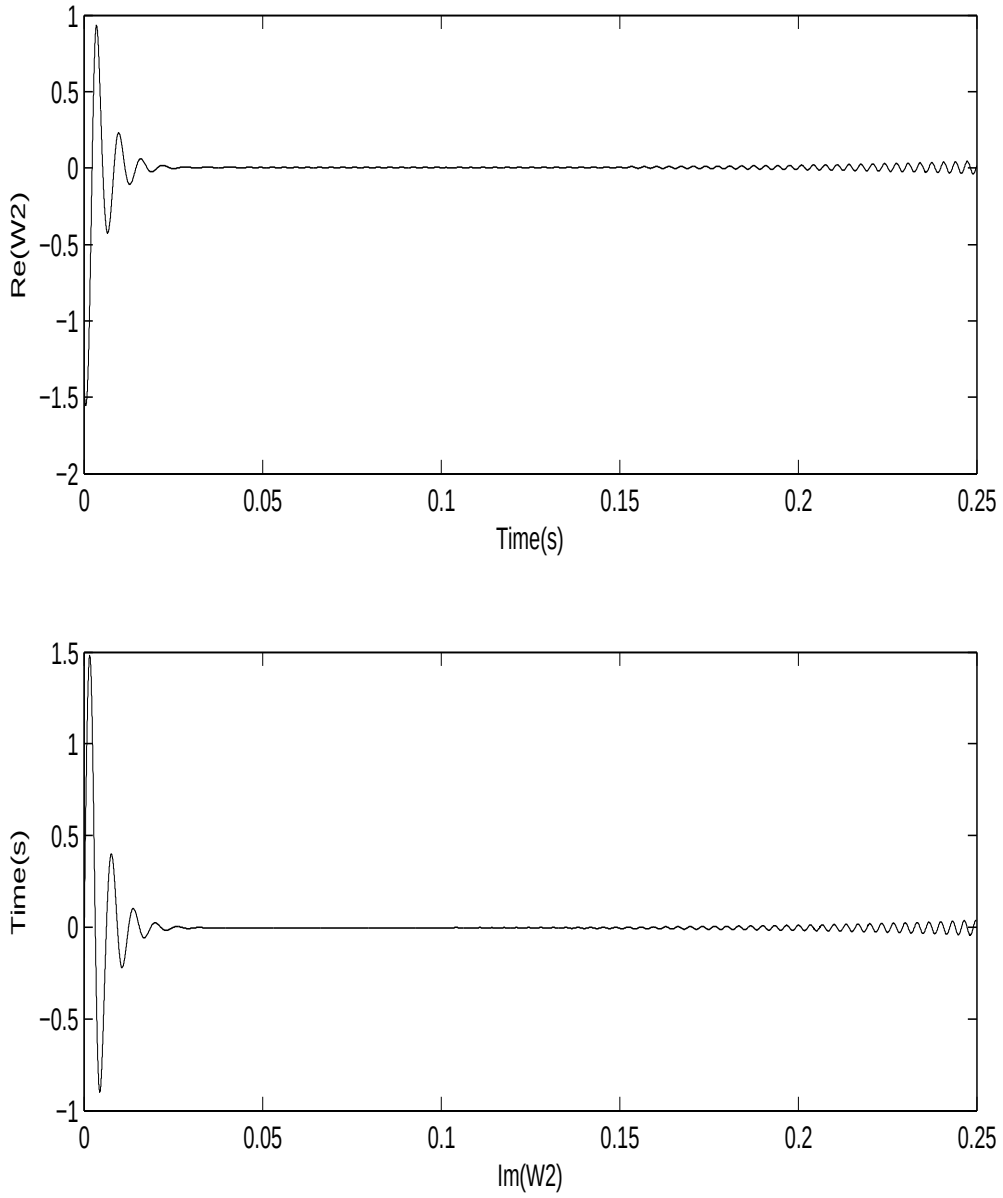

Figure 16. 2^{nd} order harmonic speed with 20% demagnetization fault

Figure 17. shows the fundamental rotor speed affected by the demagnetization fault. Once the demagnetization fault occurs, the load torque still the same, the field excitation of the rotor is decreased, thus, the electromagnetic torque decreased where the rotor speed decreased. The demagnetization occurs from t=0.1s to t=0.15s, the fundamental rotor speed decreases 6% in this region. After the fault cleared, the motor runs back to the rated speed at 326 rad/s.

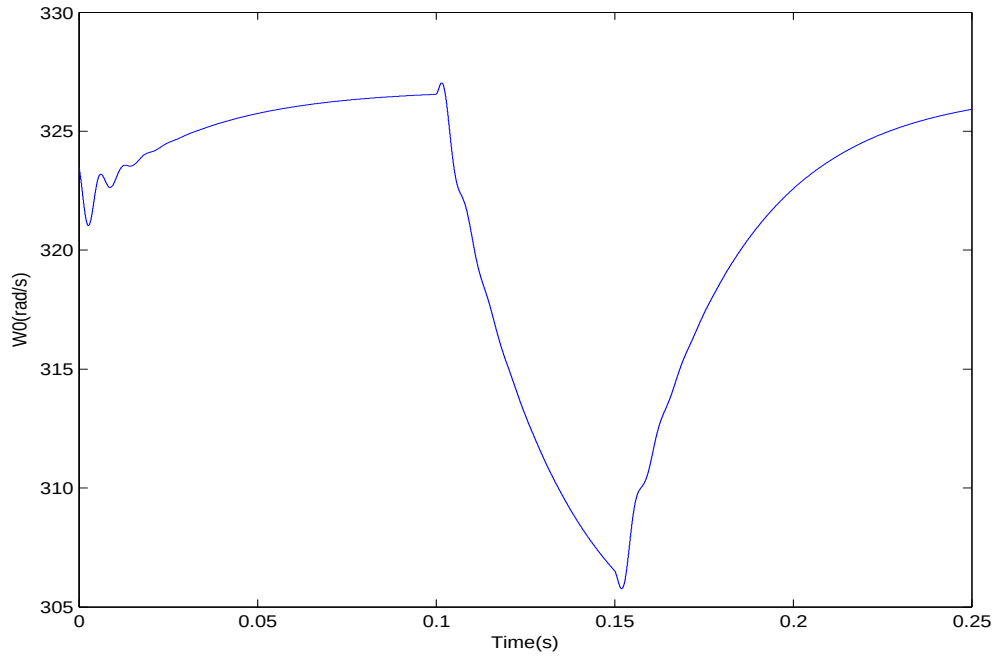

Figure 17. Fundamental rotor speed Ω_0 with 20% demagnetization fault

In the figures shown above, all the state variables are shown to observe the effect on the demagnetization faults, and all the values are shown reasonable curves. In Figure 18., the positive sequence currents are compared under 20%,40% demagnetization faults. The demagnetization faults happened at t=0.1s. As mentioned before, the armature current increased due to the demagnetization fault.

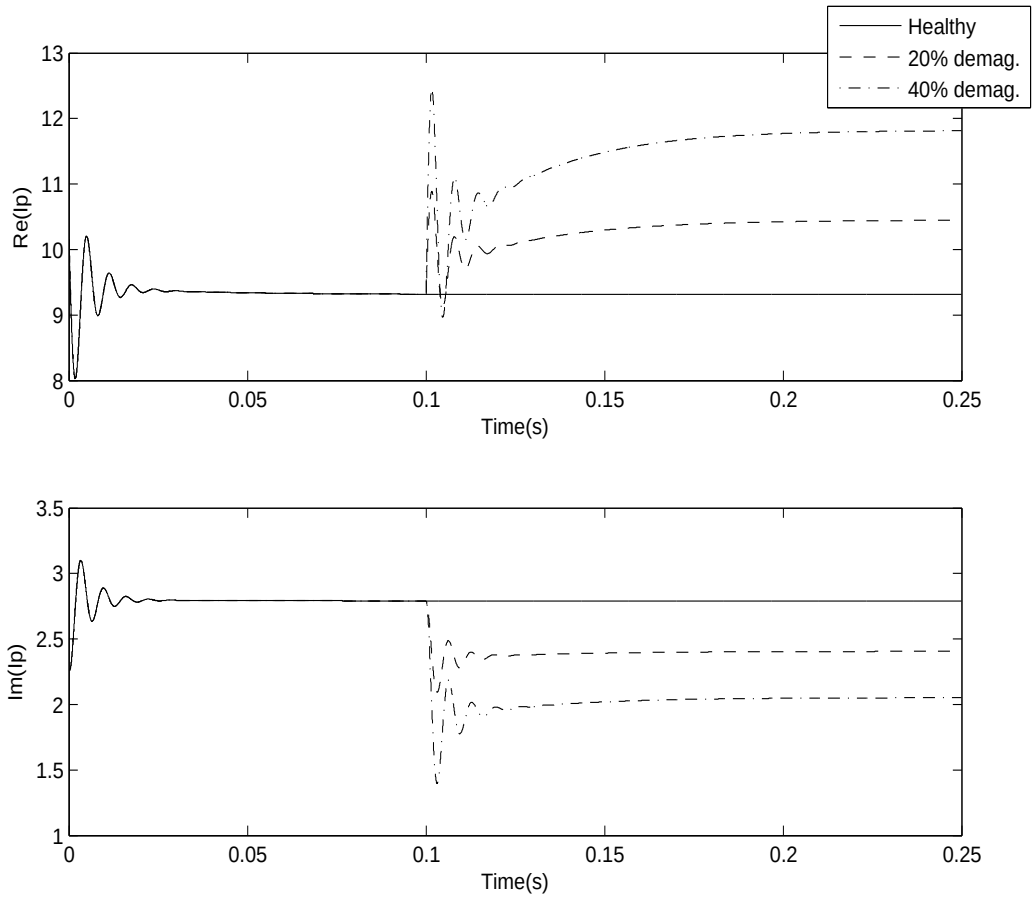

Figure 18. Comparison of $Re(I_p)$ between 20%, 40% demagnetization and healthy

Figure 19. shows the transients of negative current under 20%,40% demagnetization faults, as expected, the negative current has very little change due to the uniform demagnetization.

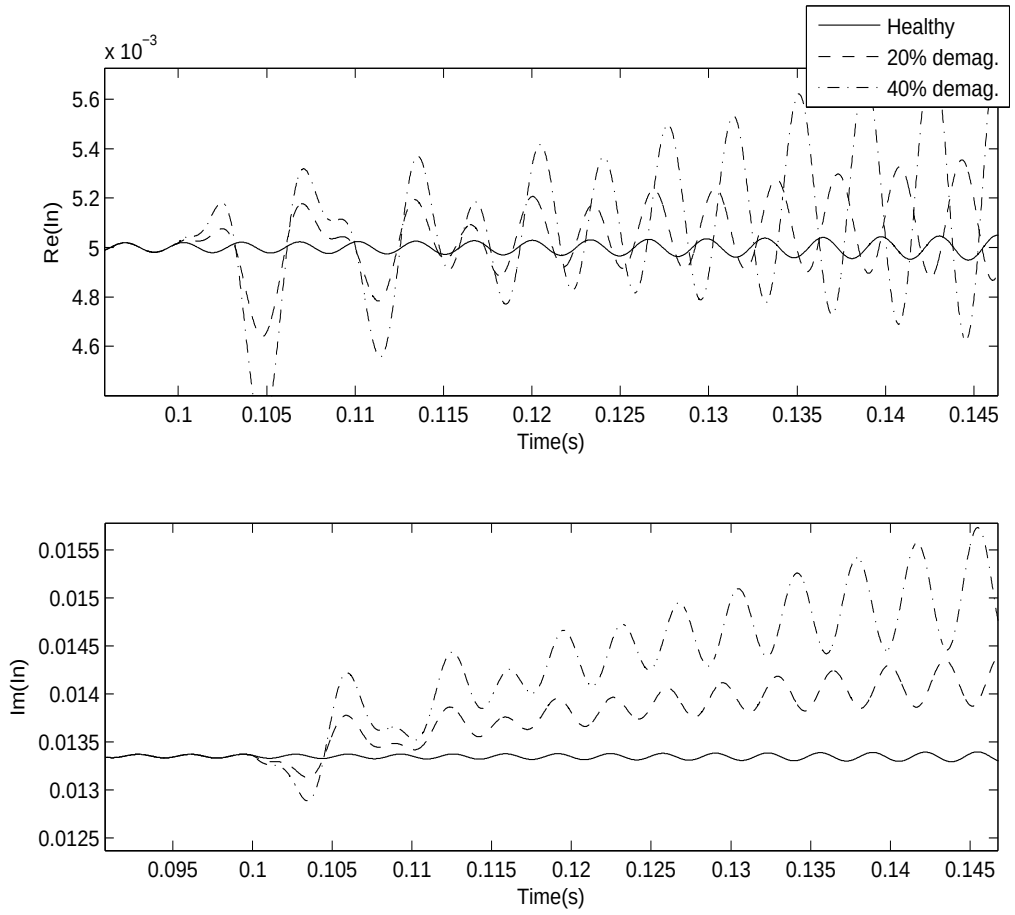

Figure 19. Comparison of $Im(I_p)$ between 20%, 40% demagnetization and healthy

Figure 20. shows the transients of rotor speed Ω_0 under different demagnetization fault levels at t=0.1s. The rotor speed is decreased more when higher level demagnetization fault occurs. 40% demagnetization causes 14% lost of the fundamental rotor speed, where 20% demagnetization causes 6% speed lost.

It need to be noted, in the simulation of dynamic phasors model system, there is no controller designed for it, so that the negative sequence current might goes to unstable with very large percentage of demagnetization.

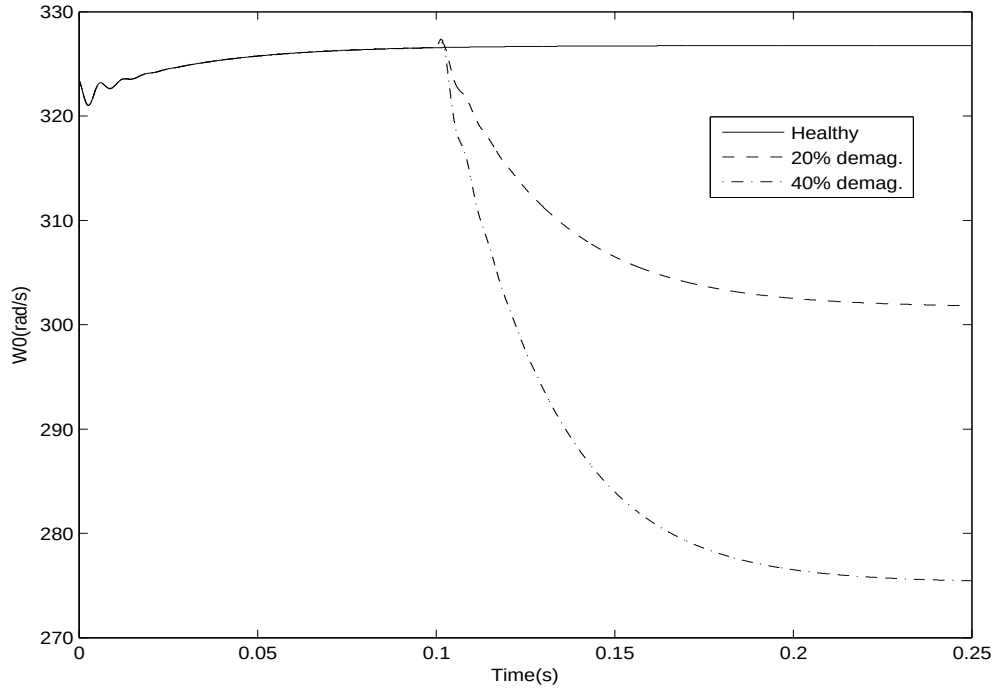

Figure 20. 20%, 40% demagnetization and healthy rotor speed Ω_0 comparison

All the figures above in this section gave reasonable results, due to the reduction of field excitation, the rotor speed decreased and same as the armature currents. Negative sequence current shows very little effect because the motor is still running balanced. Since there is no feedback loop control system in the dynamic phasors model, thus with a very large demagnetization fault or any large disturbance, the result values may goes to unstable. However, the positive sequence current a the most stabilized one.

5.2. The Effects of Grounded Faults to the Dynamic Phasors Model

Grounded fault is also one of the major faults in power systems, there are two main kinds of grounded faults, three-phase grounded fault and single phase grounded. These two faults are also simulated to in dynamic phasors model in the following figures.

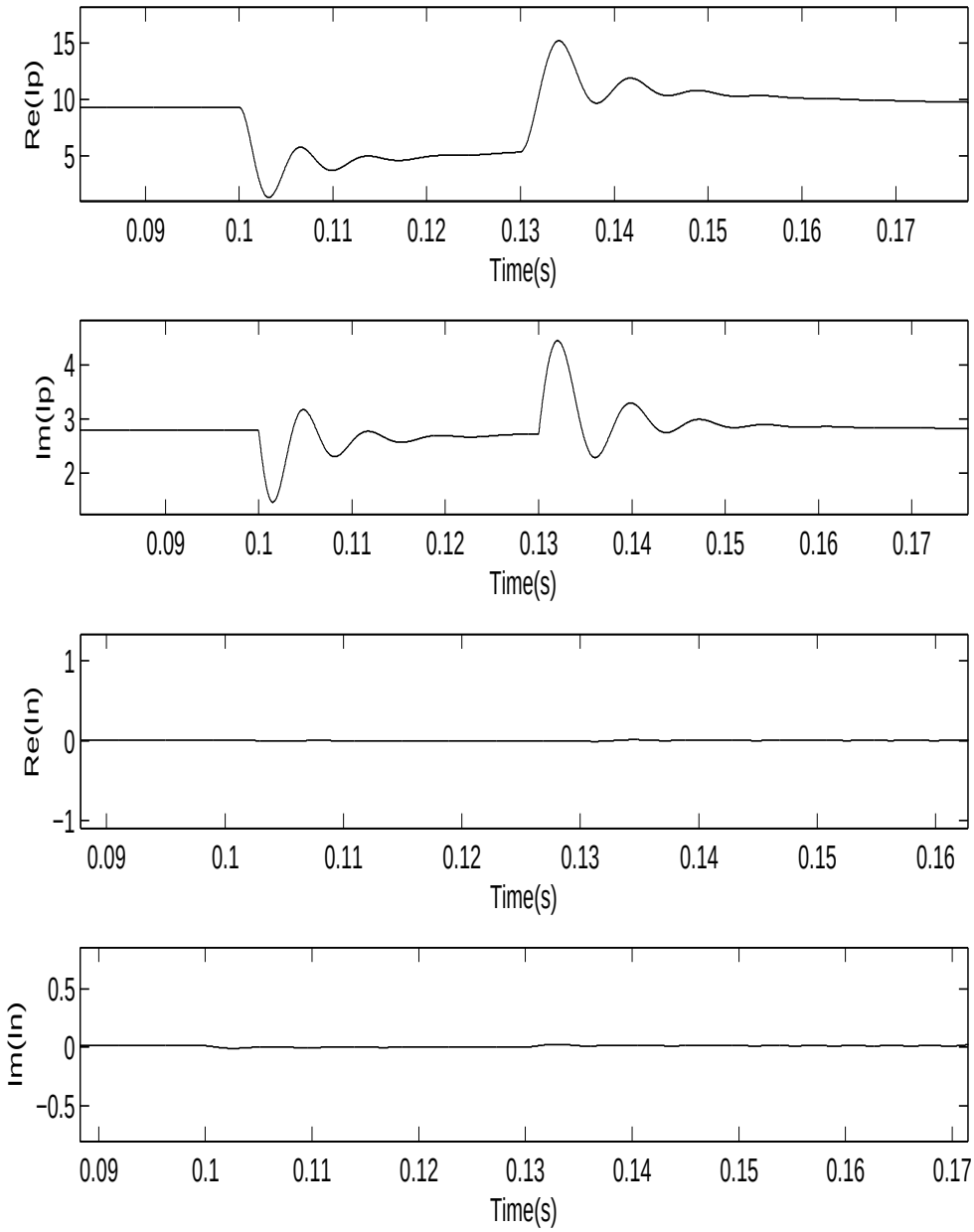

Figure 21. Positive and negative sequence currents with three-phase grounded

The positive sequence current decreased due to the lack of supply power, and negative sequence current is around zero under balanced situation. In Figure 22. a

single phase grounded fault occurs between t=0.1s to t=0.13s.

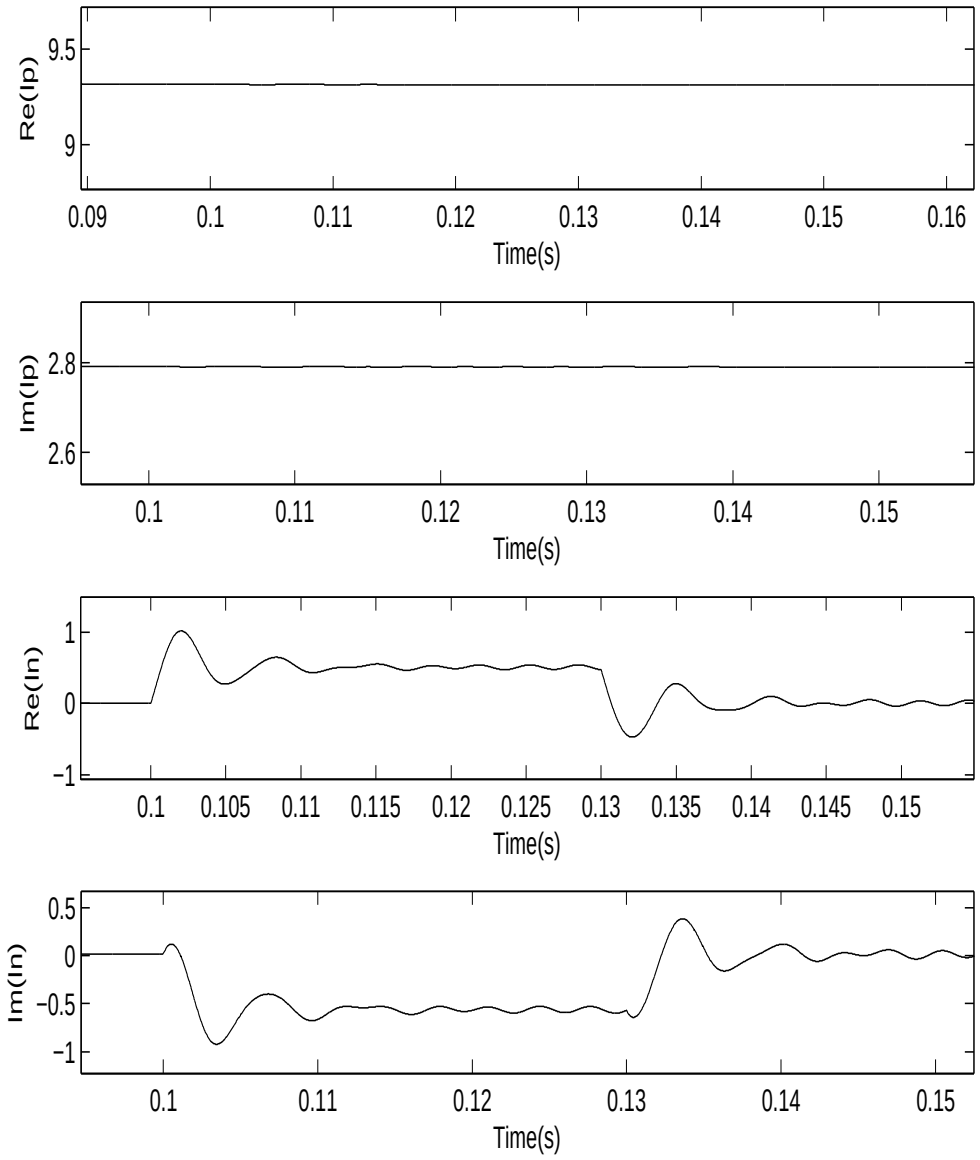

Figure 22. Positive and negative sequence currents with single-phase grounded

5.3. Comparison of Conventional IPMSM and Dynamic Phasors Model

To compare the conventional IPMSM and dynamic phasors models, the rotor frame dq0 model (26) is used as conventional IPMSM model. By using Park's transform, the three-phase (abc) current output can obtained. Substituting the three-phase current into equation (10), the positive and negative sequence currents can be obtained. As before, the positive and negative sequence currents are shown in stationary situation as in Figure 23. It can be seen the noise of the conventional model is larger than the dynamic phasors model, this may affect the accuracy when modeling the demagnetization faults due to the inaccuracy of the indicators.

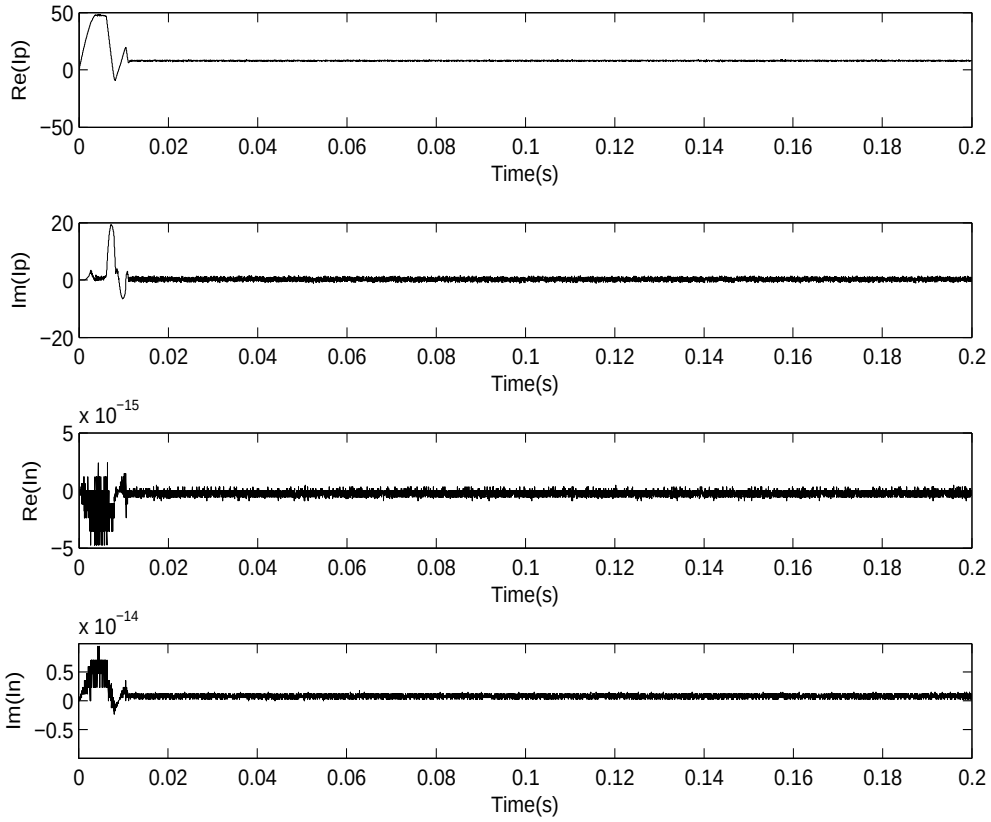

Figure 23. Positive and negative sequence currents of conventional IPMSM model

This IPMSM model is running at 325.5 rad/s with full-loaded, and the rotor speed is shown in Figure 24.

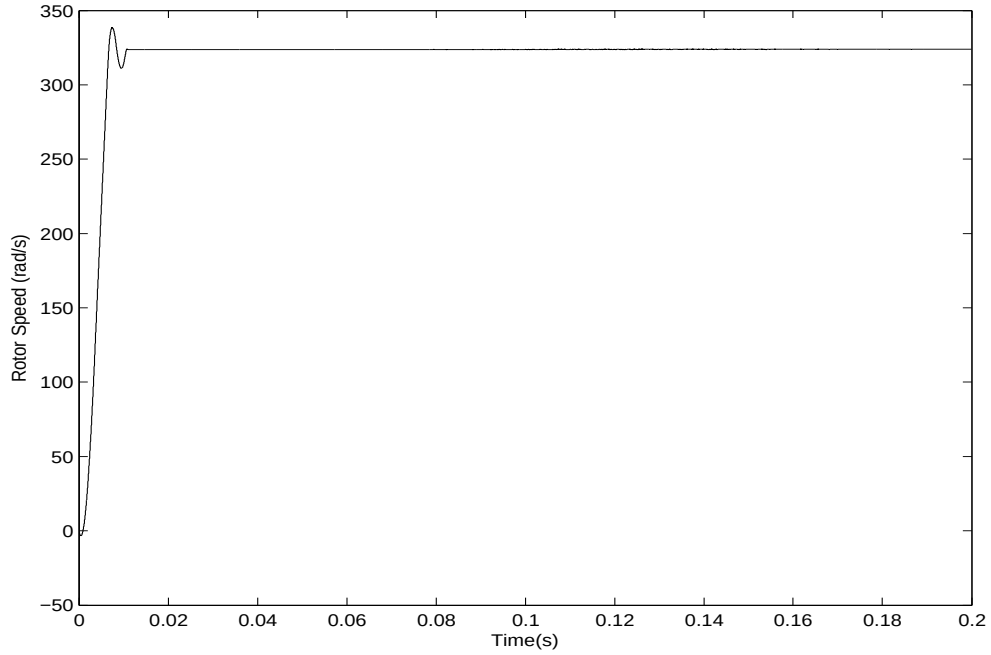

Figure 24. Rotor speed of conventional IPMSM model

To compare the conventional and dynamic phasors models, the positive sequence current will be first considered. From t=0.1s to t=0.15s, the motor has a 20% demagnetization fault. Figure 25. shows the comparison between the real part of both positive sequence currents. In Figure 25., the positive sequence current of dynamic phasors model is very close to conventional IPMSM model. We can see the current at stationary condition (before t=0.1s), both currents are around 9.5A, and after the fault occurs (after t=0.1), the currents settle down to 11.8A. This comparison shows that the dynamic phasors model consists to the conventional model with less noise, and the clear transient.

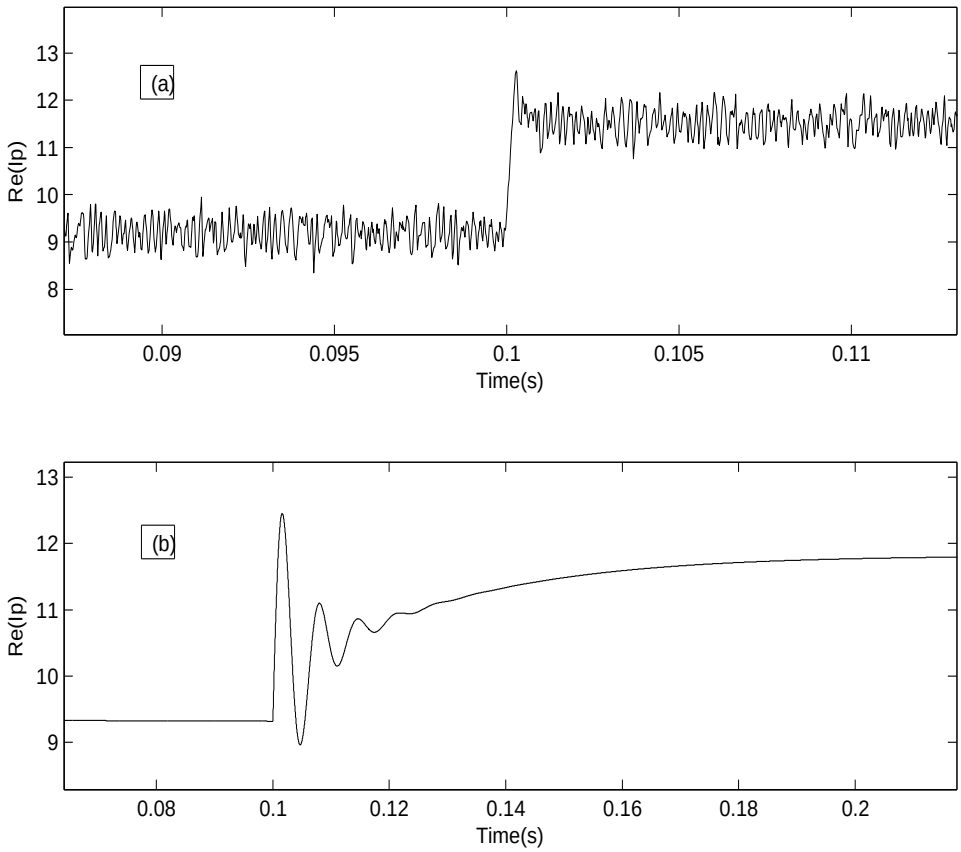

Figure 25. Positive sequence current. (a). Conventional. (b). Dynamic phasors model

We can see the conventional model in Figure 25(a)., the current values have almost 50% noise, this may cause the inaccuracy of motor fault detection, and the dynamic phasors model in Figure 25(b). shows clear change and less noise. The negative sequence current in both models are around zero, so the plots of negative sequence currents are neglected here. Since the conventional model been used in this thesis has a speed controller to ensure the motor runs in stationary condition, thus the effects caused by demagnetization fault can not be found from rotor speed.

One more important feature of dynamic phasors model, the simulation time by using MATLAB is shorter than conventional dq0 models. For the simulation of Figure 25., the conventional models cost 5.67s to finish the simulation, but in dynamic phasors model, the simulation time is only 0.22s. This is the significant increasing of efficiency in modeling and simulating in all the systems.

CHAPTER 6. CONCLUSION

6.1. Summary of Contributions

The modeling and simulation of HEV traction system is one of the most important procedures in developing the HEV systems. Nowadays, the usages of interior permanent magnet synchronous motor in electric vehicles are increasing rapidly. However, the demagnetization is one of the major concerns in designing the traction systems. The objective of this thesis is to analyze the effects of demagnetization fault of implemented interior permanent magnet synchronous motor by using dynamic phasors model. The main contributions provided by this thesis are listed below.

- The theory and key properties of dynamic phasors are outlined and explained, and the IPMSM dynamic phasors model is derived from complex space vector IPMSM model.

- Based on the operating point theory of the IPMSM, an effective method for modeling the demagnetization fault is proposed. This demagnetization fault model is used in both conventional model and dynamic phasors model.

- The dynamic phasors model of IPMSM is verified the stability by using small-signal analysis, and the eigenvalues of both faulted and healthy motors are shown and compared.

- The time domain transients of dynamic phasors model are shown, additionally, the model transients with demagnetization fault are compared to the conventional IPMSM model.

The proposed dynamic phasors model has shown the advantage on shortening computing time over the conventional IPMSM model from 5.67s to 0.22s in one certain case, and the signals of dynamic phasors model are more suitable for fault detection

since the indicators should be highly reliable. Additionally, the analysis in this thesis shows high accuracy and efficiency of dynamic phasors model. The major effects of demagnetization fault appear to the positive sequence current are reasonable. The negative sequence current has transients once the motor runs out of the balanced. The fundamental rotor speed Ω_0 is also showing the rotor speed correct when the torque ripples is small (2^{nd} order harmonic speed is around zero). To protect the IPMSM from demagnetization, it is important to keep rotor speed and load under the rated values, or the high armature current will cause the demagnetization since the high temperature.

6.2. Future Work

The purpose of this thesis is to provide an initial starting point for research into modeling the effects of demagnetization fault in interior permanent magnet synchronous motor using the dynamic phasors model. There are many other directions can be involved by using dynamic phasors models.

- In this thesis, the dynamic phasors model neglects the effect of flux linkage saturation and also the core losses. By considering these two components may improve the accuracy to the reality permanent magnet synchronous motor.

- The influence of temperature on the permanent magnet is also neglected, but there is an approximately expression as [33]

$$B_r(T) = B_r(T_0)[1 + \Delta_B(T - T_0)] \tag{48}$$

  where T is the magnet operation temperature, T_0 is the preferred temperature, $B_r(T_0)$ is the remanence at T_0, and Δ_B is the reversible temperature coefficient. By considering about the influence of temperature of the magnet will as well improve the accuracy to the IPMSM in reality.

- Eccentricity fault is also one of the major problems in IPMSM, and it is not easy to be found by many of the detection methods. Eccentricity in a machine is a condition of uneven air-gap between the stator and the rotor, this may cause the contact of stator and rotor [34]. The eccentricity fault looks very similar to demagnetization fault by using MCSA method. The patterns of the spectrum are similar to each other during these two faults. Thus, to be more powerful in modeling and simulating the faults of IPMSM, the ability to distinguish eccentricity and demagnetization must be included.

REFERENCES

[1] M. Karamuk, "A survey on electric vehicle powertrain systems," in *Electrical Machines and Power Electronics and 2011 Electromotion Joint Conference (ACEMP), 2011 International Aegean Conference on*, Sept 2011, pp. 315–324.

[2] M. Ehsani, Y. Gao, and J. Miller, "Hybrid electric vehicles: Architecture and motor drives," *Proceedings of the IEEE*, vol. 95, no. 4, pp. 719–728, April 2007.

[3] M. Zeraoulia, M. Benbouzid, and D. Diallo, "Electric motor drive selection issues for hev propulsion systems: A comparative study," *Vehicular Technology, IEEE Transactions on*, vol. 55, no. 6, pp. 1756–1764, Nov 2006.

[4] G. Nanda and N. Kar, "A survey and comparison of characteristics of motor drives used in electric vehicles," in *Electrical and Computer Engineering, 2006. CCECE '06. Canadian Conference on*, May 2006, pp. 811–814.

[5] M. Ehsani, Y. Gao, and S. Gay, "Characterization of electric motor drives for traction applications," in *Industrial Electronics Society, 2003. IECON '03. The 29th Annual Conference of the IEEE*, vol. 1, Nov 2003, pp. 891–896 vol.1.

[6] D. Casadei, F. Filippetti, C. Rossi, and A. Stefani, "Magnets faults characterization for permanent magnet synchronous motors," in *Diagnostics for Electric Machines, Power Electronics and Drives, 2009. SDEMPED 2009. IEEE International Symposium on*, Aug 2009, pp. 1–6.

[7] A. Kumar and M. Sinha, "A new burg method based approach to mcsa for broken rotor bar detection," in *Power Electronics, Drives and Energy Systems (PEDES), 2012 IEEE International Conference on*, Dec 2012, pp. 1–4.

[8] R. Schoen, T. Habetler, F. Kamran, and R. Bartfield, "Motor bearing damage detection using stator current monitoring," *Industry Applications, IEEE Transactions on*, vol. 31, no. 6, pp. 1274–1279, Nov 1995.

[9] W. le Roux, R. Harley, and T. Habetler, "Detecting rotor faults in permanent magnet synchronous machines," in *Diagnostics for Electric Machines, Power Electronics and Drives, 2003. SDEMPED 2003. 4th IEEE International Symposium on*, Aug 2003, pp. 198–203.

[10] B.-M. Ebrahimi and J. Faiz, "Feature extraction for short-circuit fault detection in permanent-magnet synchronous motors using stator-current monitoring," *Power Electronics, IEEE Transactions on*, vol. 25, no. 10, pp. 2673–2682, Oct 2010.

[11] "Detection and classification of induction motor faults using motor current signature analysis and multilayer perceptron," in *Power Engineering and Optimization Conference (PEOCO), 2014 IEEE 8th International*, March 2014, pp. 35–40.

[12] A. Khlaief, M. Boussak, and A. Chaari, "A real-time open phase faults detection for ipmsm drives based on discrete fourier transform phase analysis," in *Electrical Engineering and Software Applications (ICEESA), 2013 International Conference on*, March 2013, pp. 1–6.

[13] H. Arabaci and O. Bilgin, "The detection of rotor faults by using short time fourier transform," in *Signal Processing and Communications Applications, 2007. SIU 2007. IEEE 15th*, June 2007, pp. 1–4.

[14] L. Desheng, Y. Beibei, Z. Yu, and S. Jinping, "Time-frequency analysis based on bldc motor fault detection using hermite s-method," in *Computer Science*

and Automation Engineering (CSAE), 2012 IEEE International Conference on, vol. 2, May 2012, pp. 592–596.

[15] J.-R. Riba Ruiz, J. Rosero, A. Espinosa, and L. Romeral, "Detection of demagnetization faults in permanent-magnet synchronous motors under nonstationary conditions," *Magnetics, IEEE Transactions on*, vol. 45, no. 7, pp. 2961–2969, July 2009.

[16] S. Rajagopalan, J. Aller, J. Restrepo, T. Habetler, and R. Harley, "Analytic-wavelet-ridge-based detection of dynamic eccentricity in brushless direct current (bldc) motors functioning under dynamic operating conditions," *Industrial Electronics, IEEE Transactions on*, vol. 54, no. 3, pp. 1410–1419, June 2007.

[17] K. Moin Siddiqui and V. K. Giri, "Broken rotor bar fault detection in induction motors using wavelet transform," in *Computing, Electronics and Electrical Technologies (ICCEET), 2012 International Conference on*, March 2012, pp. 1–6.

[18] J. Rosero, A. Garcia, J. Cusido, L. Romeral, and J. Ortega, "Fault detection by means of hilbert huang transform of the stator current in a pmsm with demagnetization," in *Intelligent Signal Processing, 2007. WISP 2007. IEEE International Symposium on*, Oct 2007, pp. 1–6.

[19] J. Hong, D. Hyun, T. june Kang, S.-B. Lee, C. Kral, and A. Haumer, "Detection and classification of rotor demagnetization and eccentricity faults for pm synchronous motors," in *Energy Conversion Congress and Exposition (ECCE), 2011 IEEE*, Sept 2011, pp. 2512–2519.

[20] G. Kliman, W. Premerlani, R. Koegl, and D. Hoeweler, "A new approach to on-line turn fault detection in ac motors," in *Industry Applications Conference,*

1996. Thirty-First IAS Annual Meeting, IAS '96., Conference Record of the 1996 IEEE, vol. 1, Oct 1996, pp. 687–693 vol.1.

[21] J. Urresty, J.-R. Riba Ruiz, M. Delgado, and L. Romeral, "Detection of demagnetization faults in surface-mounted permanent magnet synchronous motors by means of the zero-sequence voltage component," *Energy Conversion, IEEE Transactions on*, vol. 27, no. 1, pp. 42–51, March 2012.

[22] P. Zhang, J. R. Marti, and H. Dommel, "Induction machine modeling based on shifted frequency analysis," *Power Systems, IEEE Transactions on*, vol. 24, no. 1, pp. 157–164, Feb 2009.

[23] D. Patel and M. Chandorkar, "Small-signal transient analysis of induction machines with stator inter-turn faults using dynamic phasors," in *Energy Conversion Congress and Exposition (ECCE), 2012 IEEE*, Sept 2012, pp. 3008–3015.

[24] A. Stankovic, B. Lesieutre, and T. Aydin, "Modeling and analysis of single-phase induction machines with dynamic phasors," *Power Systems, IEEE Transactions on*, vol. 14, no. 1, pp. 9–14, Feb 1999.

[25] R. Krishnan, *Electric Motor Drives Modeling, Analysis, and Control*. Blacksburg,VA: Pearson Education, 2012.

[26] ——, *Permanent Magnet Synchronous and Brushless DC Motor Drive*. Blacksburg,VA: CRC Press, 2010.

[27] T.J.E.Miller, *Brushless Permanent-Magnet and Reluctance Motor Drive*. London, U.K.: Clarendon Press, 1989.

[28] I. Boldea, L. Tutelea, and C. Pitic, "Pm-assisted reluctance synchronous motor/generator (pm-rsm) for mild hybrid vehicles: electromagnetic design,"

Industry Applications, IEEE Transactions on, vol. 40, no. 2, pp. 492–498, March 2004.

[29] P. C. Sen, *Principles of Electric Machines and Power Electronics, 2nd.* NewYork,U.S.: John Wiley and Sons, 1997.

[30] S. Sanders, J. Noworolski, X. Liu, and G. C. Verghese, "Generalized averaging method for power conversion circuits," *Power Electronics, IEEE Transactions on*, vol. 6, no. 2, pp. 251–259, Apr 1991.

[31] A. Stankovic, S. Sanders, and T. Aydin, "Dynamic phasors in modeling and analysis of unbalanced polyphase ac machines," *Energy Conversion, IEEE Transactions on*, vol. 17, no. 1, pp. 107–113, Mar 2002.

[32] T. Sebastian and G. Slemon, "Transient modeling and performance of variable-speed permanent-magnet motors," *Industry Applications, IEEE Transactions on*, vol. 25, no. 1, pp. 101–106, Jan 1989.

[33] Y. Da, X. Shi, and M. Krishnamurthy, "A new approach to fault diagnostics for permanent magnet synchronous machines using electromagnetic signature analysis," *Power Electronics, IEEE Transactions on*, vol. 28, no. 8, pp. 4104–4112, Aug 2013.

[34] C. Kral, T. Habetler, and R. Harley, "Detection of mechanical imbalances of induction machines without spectral analysis of time-domain signals," *Industry Applications, IEEE Transactions on*, vol. 40, no. 4, pp. 1101–1106, July 2004.